

Land use changes before and after the nuclear accident near Chornobyl city

Pedro dos Santos Ramos Magalhães Lopes
Mestrado em Ecologia e Ambiente
Departamento de Biologia
2022-2023

Orientador
Neftalí Sillero, PHD, CICGE

Coorientador
Ana Cláudia Teodoro, PHD, ICT
Zbyszek Boratyński, PHD, CIBIO/InBio


U.PORTO
FACULDADE DE CIÊNCIAS
UNIVERSIDADE DO PORTO

Acknowledgements

This work symbolises the conclusion of another cycle in my academic path, and with it comes the opportunity to recognize those who assisted me in accomplishing this achievement.

I would like to express my deepest gratitude to Professor Neftalí Sillero for accepting me in this project. His kindness, availability, and support throughout the year were unparalleled.

I'd also like to thank my co-supervisors, Professor Ana Cláudia Teodoro and Professor Zbyszek Boratyński, for sharing their knowledge and assisting with the research and any challenges that arose along the way. They were all very kind and I will forever be grateful.

I am thankful to the staff of the Observatório Astronómico Prof. Manuel de Barros for welcoming me and providing the resources necessary for my research, and to my colleagues working there, for the help and insight they provided during my work.

Finally, I would like to thank my family and friends for the support they gave me during these past few years. Without them this would surely not be possible.

Resumo

O acidente nuclear próxima da cidade de Chornobyl (Ucrânia) é um dos dois acidentes classificados com gravidade máxima na Escala Internacional de Eventos Nucleares, juntamente com o acidente perto de Fukushima em 2011 (Japão). No dia 26 de Abril de 1986 explodiu o reator nuclear nº4 levando à maior libertação de produtos radioativos na história da indústria nuclear civil para a atmosfera. Durante dez dias foram libertadas enormes quantidades de iodo-131 e de césio-137 (assim como outras partículas perigosas em menores quantidades). Apesar de muito deste material se ter depositado nas imediações da central, os materiais mais leves foram espalhados pelo vento pela Ucrânia e Bielorrússia, e maior parte da Europa. Trinta-e-seis horas após o acidente, foi designada uma zona de exclusão de 10 km da qual foram evacuadas todas as pessoas assim como animais de estimação. Contudo, devido a uma contaminação muito maior, a zona de exclusão foi aumentada de 10 para 30 km. A evacuação gerou um abandono completo dos terrenos dentro da zona de exclusão. O objetivo do presente estudo é analisar com técnicas de deteção remota, alterações espaciais e temporais que ocorreram devido a esta drástica alteração nos usos do solo dentro da Zona de Exclusão de Chornobyl após o acidente. Para o estudo em questão foram selecionadas imagens do satélite Landsat de 5 em 5 anos a partir do ano do incidente, procedendo-se à sua classificação com o QGIS e o Semi-Automatic Classification Plugin. Foram classificadas duas imagens por ano, com exceção de algumas imagens cuja classificação não era possível devido à baixa qualidade ou elevada presença de nuvens da mesma. Um total de 15 imagens foram classificadas, divididas em dois grupos – com foliação e sem foliação. Os resultados mostram uma sucessão natural da vegetação, notando-se especialmente o decréscimo de campos agrícolas ao longo dos anos em contraste com um aumento da vegetação geral. O abandono do território teve um impacto positivo na recuperação da vegetação (sucessão natural), superando na generalidade os impactos da radiação.

Palavras-chave: Chornobyl, radiação, vegetação, alterações, QGIS, Landsat.

Abstract

The nuclear accident near Chornobyl City (Ukraine) is one of the two accidents classified as a Major accident on the International Scale of Nuclear Events, along with the accident near Fukushima in 2011 (Japan). On April 26th, 1986 the nuclear reactor nº 4 exploded leading to the biggest release of radioactive products into the atmosphere in the history of the civil nuclear industry. For ten days huge quantities of iodine-131 and cesium-137 were released (as well as other dangerous particles in smaller amounts). Despite the deposition of a huge amount of this material near the central, the lightest materials were scattered by the wind across Ukraine and Belarus, and most of Europe. Thirty-six hours after the accident an exclusion zone of 10 km was designated, evacuating from there all people and domestic animals. However, due to a much wider contamination, the exclusion zone suffered an increase from 10 to 30 km. The evacuation led to a complete abandonment of the land inside the exclusion zone. The objective of the current study is to analyse, through remote sensing techniques, spatial and temporal changes due to this drastic change in land use inside the Chornobyl Exclusion Zone after the accident. For the study in question images of the Landsat satellite were selected every 5 years from the year of the accident, and were classified with QGIS and the Semi-Automatic Classification Plugin. Two images were classified per year, except for some whose classification was not possible due to the low quality or high presence of clouds. A total of 15 images were classified and divided into two groups – Foliage and No Foliage. The results show a natural vegetation succession, noting especially the decrease of agricultural fields over the years in contrast to an increase in general vegetation. The abandonment of the territory had a positive impact on vegetation recovery (natural succession), mostly surpassing the impacts of radiation.

Keywords: Chornobyl, radiation, vegetation, changes, QGIS, Landsat.

Table of Contents

1. Introduction 1
1.1 Chornobyl Nuclear Power Plant 1
1.2 Chernobyl Accident 3
1.3 Ionising Radiation 5
1.4 The impact of Ionising Radiation 6
1.5 Adaptation of Vegetation to Radioactivity 8
1.6 Remote Sensing 9
1.7 Objectives 10
2. Materials and Methods 11
2.1 Area of study 11
2.2 Fieldwork and Image Treatment 12
2.3 Images Classification 13
2.3.1 The Minimum Distance Method 18
2.3.2 Validation of the classification maps 18
2.4 Temporal Analyses 18
3. Results 19
3.1 Classification 19
3.2 Global Trends 20
3.3 Local Trends 22
4. Discussion 29
5. Conclusion 32
References 33
Appendix I 40
Appendix II 44
Appendix III 48
Appendix IV 50

List of Tables

Table 1 – List of vegetation classes analysed and their description. 15

Table 2 - Summary Statistics Table for the Foliage dataset. 21

Table 3 - Summary Statistics Table for the No Foliage dataset. 21

Table 4 - Results of the ANOVA Test. SS - Sum of Squares - quantifies the variability between or within the groups; df - degrees of freedom; MS - Mean Square - average variation either between or within the groups; F - statistical test used in one-way ANOVA; P-value indicates whether to accept the null hypothesis or the alternative hypothesis; F critical value indicates if the test is significant..... 22

Table 5 - Results of the Mann-Kendall and p-value tests and Sen´s Slope value of the Foliage dataset. The Sen's Slope values indicate the type of trend. Positive numbers indicate positive trends; negative values indicate negative trends; and zero indicates no trend (neutral). 22

Table 6 - Results of the Mann-Kendall and p-value tests and Sen´s Slope value of the No Foliage dataset. The Sen's Slope values indicate the type of trend. Positive numbers indicate positive trends; negative values indicate negative trends; and zero indicates no trend (neutral). 23

List of Figures

Figure 1 – Uppermost position of a control rod of the RBMK emergency protection system relative to the reactor core (a) before and (b) after the improvements made in response to the Chernobyl accident. Dimensions are given in centimetres (by Anon., 1992, accessed: Feb 2023)..... 2

Figure 2– A light Water Graphite-moderated Reactor (LWGR/RBMK) (by world-nuclear.org, accessed: Feb 2023)..... 3

Figure 3 – The destroyed Unit-4 reactor (top view) (by Imanaka 2002, accessed: March 2023). 4

Figure 4 – Types of radiation and respective penetrating power (by world-nuclear.org, accessed: March 2023)..... 5

Figure 5 – Irradiated and damaged forest stands so-called “red forest” located within the territory of the 10-km zone around the Chornobyl nuclear power plant. The picture was taken in October 1997 by W. Wloch. (By Tulik & Rusin 2005, accessed: April 2023). 11

Figure 6 - Close-up of 3 sampled locations (red) inside the 30 km CEZ from the year 2017. 13

Figure 7 – Landsat satellite image from Chornobyl Nuclear Power Plant from the year 1984, contaminated with clouds. 14

Figure 8 - 1986 and 2017 Foliage Season classification maps..... 18

Figure 9 - 1990 and 2017 No Foliage Season classification maps 18

Figure 10 - Progression of the landscape change in Chornobyl over the course of a year during the Foliage phase. The y-axis represents the number of pixels in the classified photographs and how they evolved throughout the years. 19

Figure 11 - Progression of the landscape change in Chornobyl over the course of a year during the No-Foliage phase. The y-axis represents the number of pixels in the classified photographs and how they evolved throughout the years. Although both graphs' y-axes terminate in 2017 (the year the information was obtained), the graphic from the No-Foliage period begins in 1990 since there were no suitable photos from the year of the accident. 20

Figure 12 - Foliage dataset Sen’s Slopes of the Pines, Grassland, Betula, Alder, Oak and Robinia pseudoacacia classes 24

Figure 13 - Foliage dataset Sen's Slopes of the Marshland, Robinia, Field, Mixed, Grassland Trees and Deciduous Forest classes 25
Figure 14 - No Foliage dataset Sen's Slopes of the Pines, Grassland, Betula, Alder, Oak and Robinia pseudoacacia classes..... 26
Figure 15 - No Foliage dataset Sen's Slopes of the Marshland, Robinia, Field, Mixed, Grassland Trees and Deciduous Forest classes 27

List of Abbreviations

BWR - Boiling Water Reactor

CEZ - Chornobyl Exclusion Zone

DNA - Deoxyribonucleic Acid

ECCS -Emergency Core Cooling System

EM - Electromagnetic

FCUP – Faculty of sciences of the university of Porto

GPS - Geographic Positioning System

GIS - Geographic Information System

IR – Ionising Radiation

LWGR - Light Water Graphite Reactor

MDM – Minimum Distance to Mean

MW – Megawatts

NEA – Nuclear Energy Agency

ORM – Operating Required Margin

PWR - Pressurised Water Reactor

RBMK - Reaktor Bolshoy Moshchnosty Kanalny (High-power Channel Reactor)

RS - Remote Sensing

SCP - Semi-Automatic Classification Plugin

UP - University of Porto

USGS - United States Geological Survey

USSR - Union of Soviet Socialist Republics

1. Introduction

Radiation, at its core definition, is energy with wave-like properties, an electric field, and a magnetic field associated, and travels from its source, through space at the speed of light. The spontaneous release of this energy from an unstable atom occurs when this same atom achieves a more stable state and is called radioactivity or radioactive decay (L'Annunziata 2007).

The potential of this type of energy was rapidly realised soon after its weaponized use during the Second World War and peaceful applications were sought. Promptly nuclear power was branded as a pollution-free energy source that could produce nearly limitless amounts of electricity (Filburn *et al.* 2016).

Many nuclear power accidents have occurred. Some were the result of human error; others were caused by natural disasters that led to tragic outcomes. The Fukushima Dai-ichi nuclear disaster, the most recent one that happened in 2011, was the result of the latter causes (Sekizawa *et al.* 2015).

The Fukushima Dai-ichi Nuclear Power Plant was prepared to withstand an 8.9 earthquake (on the Richter scale) and a tsunami of 5.7 m in height. Unfortunately, both calamities surpassed the security measures with the earthquake of 9.0 on the Richter scale generating a 13 m tsunami that flooded all 6 units of the power plant. Despite this and because of the different positioning of each unit's backup generators, two of the units suffered less damage and thus the radioactive material was 6 to 10 times less than that released in the Chernobyl accident. Still, the damage was very severe on the other units as three of them underwent disastrous hydrogen explosions and core meltdowns (Filburn *et al.* 2016).

In opposition, the Chornobyl accident was not a result of nature’s action but rather the negligence of human nature.

1.1 Chornobyl Nuclear Power Plant

The Chornobyl nuclear power plant was composed of four Soviet-designed RMBK – Reaktor Bolshoy Moshchnosti Kanalny – reactors located on the banks of a man-made lake that provided cooling water for all the reactors and a convenient media where to inject the reactor’s waste heat. As described by Anon., 1992, this type of reactors were light water graphite reactors (LWGR) that used water as cooler and large blocks of

graphite attached to the end of the control rods, as shown in Figure 1, to moderate the reaction. The reactor core, arranged in a cylindrical shape, was 7 m tall and 11.8 m in diameter.

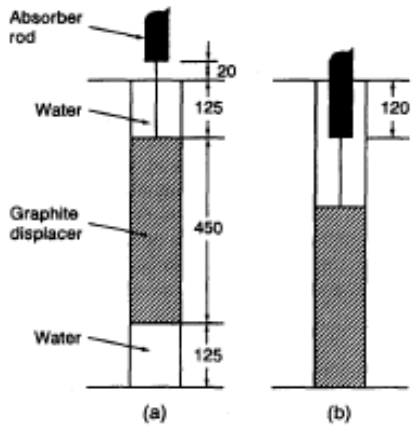


Figure 1 – Uppermost position of a control rod of the RBMK emergency protection system relative to the reactor core (a) before and (b) after the improvements made in response to the Chernobyl accident. Dimensions are given in centimetres (by Anon., 1992, accessed: Feb 2023).

Water enters the reactor core from below and, in similarity with what happens in the boiling water reactor (BWR) and in the pressurised water reactor (PWR), it starts boiling in the fuel channels and the steam generated is separated above them in a single circuit.

Fuel pellets of slightly enriched uranium oxide are enclosed in a zircaloy tube 3.65m long, forming a fuel rod. A fuel assembly contains 18 fuel rods arranged cylindrically in a carriage (Murphy 2006).

This type of reactor was only built in the Soviet Union, and it was widely used throughout the cold war as it was cheaper, faster to build and could generate high energy levels. Because of this, its design included several different features from the ones developed in Europe and North America.

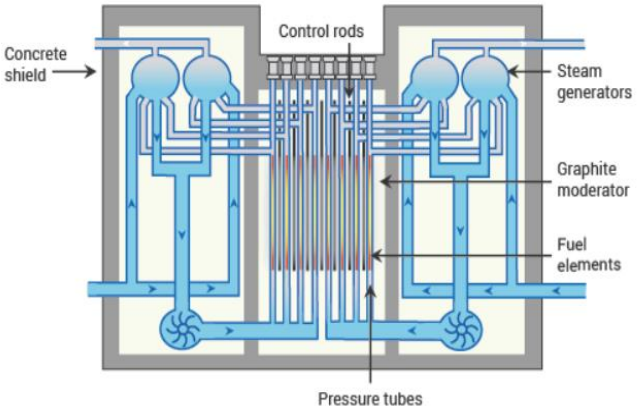


Figure 2– A light Water Graphite-moderated Reactor (LWGR/RBMK) (by world-nuclear.org, accessed: Feb 2023).

After the accident in Chornobyl, this design was deemed unsafe and safety changes were conducted to prevent similar accidents from occurring (world-nuclear.org).

1.2 Chernobyl Accident

In the 70's, as part of a large country-wide nuclear program, the former USSR built the nuclear power complex in Chornobyl (Schmid 2015; Filburn *et al.* 2016).

Its location was strategically chosen as it was located only 90 miles north of Kyiv, the perfect distance so that it could support the electrical needs of over two million people without risking their lives in case an accident occurred (Josephson 2005; Filburn *et al.* 2016).

As mentioned previously the design of the reactors in Chornobyl, and other power plants in the Soviet Union, was different from those used all around the world. Because of this, and to ensure that in case of a power failure the power requirements of the reactor would be met, a test was carried out to study the possibility of utilising the mechanical energy of a turbogenerator after a cut-off of steam supply.

At 2 PM April 25th the emergency core cooling system (ECCS) was switched off following the experiment program and an order was received from the Kyiv dispatcher of the electrical grid to maintain the operator working due to a shortage of power. From this point forward, the reactor was operated at the power of 1500 MW with the ECCS system switched off. However, a problem was created by this delay: a shift change occurred at midnight (time that the test could be resumed) and the new crew was not familiar with the procedure. At this time, the operator started to decrease power down to 720 MW,

however the core was already filled with Xenon (element formed from the split of Uranium that is toxic to the reactor core and accumulates when the reactor is working at low power) which prevented the stabilisation of power, leading it to fall to 30 MW, and therefore stalling the reactor (Medvedev 1989; Imanaka 2002).

At 1 AM April 26th the required operating margin – ORM – was violated and to raise the power for the test, almost all control rods were completely withdrawn leaving only 8 inserted. Twenty-three minutes after this, the test started. The emergency regulating valves of the second turbogenerator were closed, no water was passing through the core, and the power started to rise uncontrollably. The safety button was pressed to induce a complete shutdown of the reactor (by inserting all control rods simultaneously) but because the control rod's tips were made of graphite, they reacted with the xenon accumulated leading to the explosion of the core after 6-7 minutes (Imanaka 2002). According to Medvedev., 1989, approximately 50 tons of vaporised fuel were flung into the atmosphere.

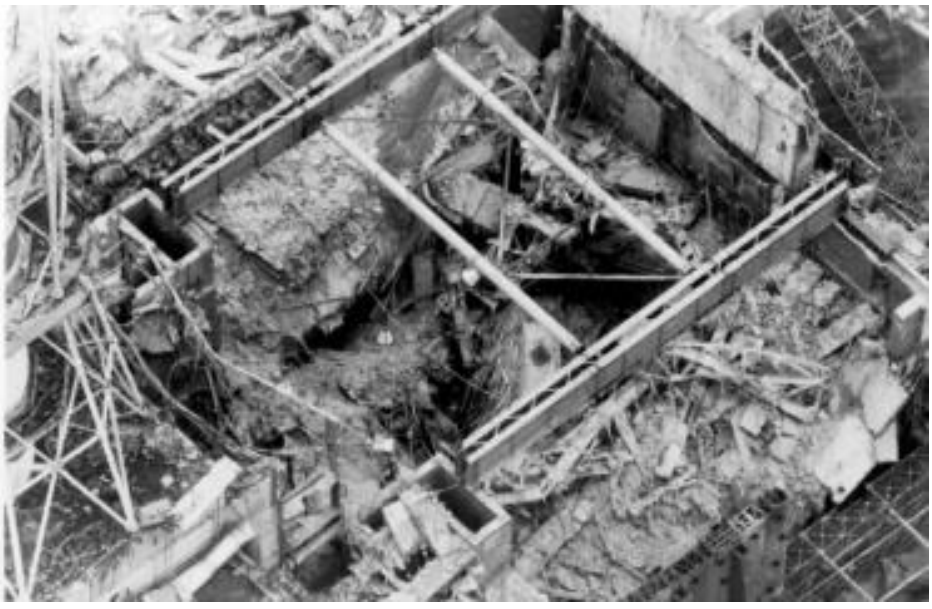


Figure 3 – The destroyed Unit-4 reactor (top view) (by Imanaka 2002, accessed: March 2023).

Over the 10 days after the accident, approximately 10^{19} Bq (Becquerel – unit of radioactivity in the International System of Units) of radionuclides was released into the air (Imanaka 2002; Santos *et al.* 2019a).

1.3 Ionising Radiation

Although ionising radiation can occur naturally (from radioactive materials and cosmic rays) and on Earth stems primarily from geological processes, being the result of the decay of radionuclides (of elements such as thorium, uranium, and radium all present in base rocks, e.g., granite), its source can also be artificial through the fuel spent in nuclear power plants (Caplin & Willey 2018b; Ludovici *et al.* 2020; Mousseau & Moller 2020).

Types of ionising radiation include alpha, beta and neutron particles that are subatomic particles with mass; and gamma rays and X-rays, high-energy electromagnetic protons with no mass and no charge (Mettler & Upton 2008). Each one has a different penetrating power (Figure 4) and can travel different distances interacting with the atoms of the materials on their paths (causing excitation or ionisation). Radiation is measured in Becquerel (Bq) defined as the activity of a quantity of a radioactive material in which one nucleus decays per second (world-nuclear.org).

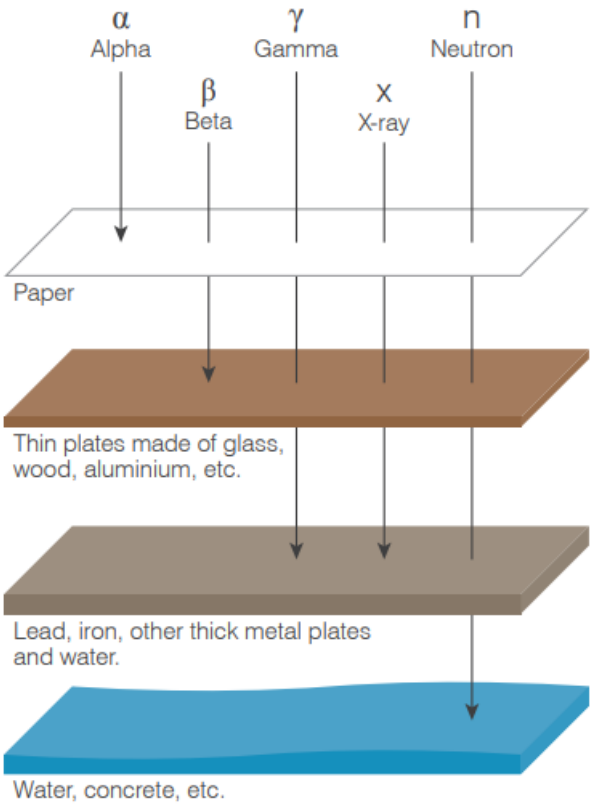


Figure 4 – Types of radiation and respective penetrating power (by world-nuclear.org, accessed: March 2023).

According to the International Atomic Energy Agency (IAEA.org) as of 2023, 437 Nuclear Power Plants are active and operating and despite being able to produce an 389.5 GWe

total net of electricity globally, a lot of nuclear waste and Ionising Radiation (IR) is also formed making it a pollutant of global significance.

Therefore, because of the accidents that we faced in the past related to Nuclear Power Plants, and because the concern radionuclides pose to human health and the environment, studies have been made to further increase our understanding on the topic and its effects in ecosystems (Dighton *et al.* 2008).

1.4 The impact of Ionising Radiation

In April 1898, just 3 years after the discovery of X-rays by Röntgen, a “Committee on X-ray Injuries” was appointed by the British Roentgen Society after observing the first adverse tissue events after exposure to IR. According to Foray *et al.* (2016), IR responses elicit three major aspects: adverse tissue events (non-cancer effects attributable to cell death, notably skin reactions); radiation-induced cancers; and non-cancer effects that are often considered attributable to mechanisms other than cell death (cataracts and circulatory disease).

The biological effects of ionising radiation have been extensively investigated over several decades, however, a significant level of uncertainty persists regarding the impact of dose rates on these effects. Usually, DNA is the primary site of radiation damage. If the dose is low many of the resulting lesions can be promptly repaired and remediated, if the dose is higher and the species being exposed to it is more radiosensitive, DNA breaks can generate both genomic and chromosomal aberrations (Bonisoli-Alquati *et al.* 2010; Ravanat *et al.* 2016; Ludovici *et al.* 2020).

Recent research, such as the study by Lowe *et al.* (2022), indicate that at low radiation dose rates, there may be potential positive cellular effects and minimal adverse genetic effects, as long as the total cumulative dose remains low. For example, radiotherapy for the treatment of cancer through ionizing radiation to target and kill tumour tissue(De Ruysscher *et al.* 2019).

Studies conducted in the Chornobyl region have primarily focused on assessing genetic and physiological effects on organisms residing in areas with elevated radiation levels. These investigations, as highlighted by Mousseau and Systematics (2021), consistently demonstrate significant injuries and reduced population abundances among various species inhabiting more radioactive zones.

Previous research have shown increased mutation rates in some, but not in all plants exposed to ionising radiation. Comprehensive studies on genetics, development, and life history at terrestrial sites rich in radionuclides provide an opportunity to experimentally investigate the consequences of long-term exposure to a wide range of ionising radiation sources (Kovalchuk *et al.* 2000; Møller & Mousseau 2013; Aguileta *et al.* 2016; Mousseau & Moller 2020).

As emphasized by Mousseau and Moller (2020), current knowledge suggests that many plant species are susceptible to genetic damage and development abnormalities when exposed to ionising radiation, which are not typically observed under "normal" conditions (average values of radiation in most environments). Field studies in Chornobyl suggest that radiation effects on decomposition may be affecting plant growth in important ways (Mousseau et al. 2014).

Amongst the several thousand clean-up workers who were sent to Chornobyl from 1986 through 1989 to mitigate the consequences of the accident, around 237 workers (mostly the emergency workers who dealt with the fires and other situations within hours of the accident) were reported to developed acute radiation sickness. Most of the workers received lower doses of radiation primarily due to external irradiation from gamma-emitting radionuclides and therefore the consequences were not as severe (Na *et al.* 2002; Hatch *et al.* 2005). Before the autumn of 1986, a total of 116,000 members of the general public were evacuated from the area within 30 km of the damaged reactor. 100,000 of those within two weeks of the accident (Hatch *et al.* 2005).

According to NEA (2002), the exposure of members of the staff of the nuclear power plant as well as nearby residents and residents of contaminated areas to radiation, as a result of the accident, resulted in two main pathways of exposure. The first is the radiation dose to the thyroid as a result of the concentration of radioiodine and similar radionuclides in the gland. The second is the whole-body dose caused largely by external irradiation, mainly from radiocesium. The absorbed dose to the whole body is thought to be 20 times more deleterious, in terms of late health effects incidence, than the same dose to the thyroid (IC90).

The releases during the Chernobyl accident contaminated about 125 000 km2 of land in Belarus, Ukraine, and Russia with radiocaesium levels greater than 37 kBq/m2 (NEA 2002). Although trees possess high filtering characteristics (resulting in much higher deposition in forests than in agricultural areas), the migration downwards of caesium in

forests and peaty soil is generally slow and because it depends on many factors such as the soil type, pH, rainfall, and agricultural tilling it is hard to understand the outcome. Because of this, large variations in the deposition levels occurred, however deposition was often higher in forests than in agricultural areas (NEA 2002).

To decontaminate the soil, various strategies were applied, such as the removal and disposal of the uppermost topsoil. Along with all the decontamination measures introduced, the land abandonment from the people was also a prominent factor in the restoration of the vegetation (NEA 2002).

1.5 Adaptation of Vegetation to Radioactivity

The effects of IR in higher plants are of interest in various areas, such as agriculture, ecology and health, and although numerous fauna and flora communities have shown resistance in radioactive contaminated sites, there are still studies that report significant effects of chronic irradiation at relatively very low doses (Ludovici *et al.* 2020).

The effects of chronic low doses on plants are not well known in comparison to the effects of acute high dose rate exposures on plant genetics, growth, and development. As such, *in situ* studies of the effect of radionuclides at nuclear accident sites (such as Chornobyl and Fukushima), atomic bomb test sites, and areas of naturally high radiation levels, could provide insights concerning the mechanisms of radiation effects on living systems (Caplin & Willey 2018a; Mousseau & Moller 2020).

The exposure of a biological system to IR can happen in two basic types of interactions: direct or indirect. In direct actions, radiation energy is deposited directly into the target; in contrast, in indirect actions, energy is absorbed by the external medium, which leads to the production of diffusible intermediates which therefore affect the targets. The main target however, in both types of interactions, is the water molecule. The primary reactions are excitation and ionisation, which produce ionised water molecules and the radicals H and OH. The OH radical can react rapidly with various types of macromolecules in particular DNA (Esnault *et al.* 2010).

Currently much more is known of the effects of ionising radiation on organisms with lower antioxidant capacity than plants (Ludovici *et al.* 2020). Whereas in animals the effects of IR can cause carcinogenesis, in plants due to the different controls on groups of multiplying plant cells (and because of the low probability of metastasis in organisms with

no circulatory systems), no carcinogenic effects similar to animals are suffered (Aktipis *et al.* 2015; Caplin & Willey 2018a).

According to Hinton *et al.* (2007), the doses that plants received from the Chernobyl disaster were mainly influenced by the physical properties of the different radionuclides (e.g. their half-lives, radiation emissions). However, the physiological state of the plant species at the time of the accident as well as the individual species-specific properties of each plant variety to absorb the radionuclides, also played an important part. In addition, given the occurrences of the accident in the middle of spring, the harmful effects of the relapse were accentuated as it coincided exactly with the period of development of the shoots and reproduction in the plants (Hinton *et al.* 2007; Garnier-Laplace *et al.* 2013; Caplin & Willey 2018a; Beresford *et al.* 2020). Despite this, indirect effects such as land abandonment by humans appear to have a significant impact on biota within the 30-km CEZ compared to radiological effects (Ludovici *et al.* 2020).

1.6 Remote Sensing

Remote sensing offers an opportunity to study and monitor land use changes (Carlson & Sanchez-Azofeifa 1999). It provides information about the Earth's surface by measuring electromagnetic (EM) energy. The most important source of EM energy at the earth's surface is the Sun and therefore, many sensors used in RS measure reflected sunlight. These types of sensors are called passive sensors; they also measure energy emitted by the Earth itself. Sensors that provide their own energy are called active sensors. (Kerle *et al.* 2004).

Remote-sensing data has a long history of being used for deriving land-cover maps, even before the launch of the first Lansat platform (1972). Aerial photography served as a primary source of information on land cover before the availability of satellite imagery (Akbari *et al.* 2003; Sohl *et al.* 2012). With the increase of global concerns, such as climate change and environmental degradation, RS has become a vital tool, and for many applications (such as the study of climate change, environmental degradation, among others) the only one suitable (Kerle *et al.* 2004).

RS information, in concert with available enabling technologies such as GPS and GIS, helps to provide cost-effective decisions and RS products. Further, increased availability and access to remote sensing data (i.e. long-term and historical), GIS, and spatial data sets from digital libraries have been an invaluable aid to the development of image

processing systems in the last decade (Franklin *et al.* 2000; Rogan & Chen 2004; Jensen 2009).

RS acquires data in a standard and continuous way, globally, using the same or a similar sensor which enables methods for monitoring and change detection (Rogan & Chen 2004).

Objects behave differently with different wavelengths of incident energy and, therefore, have unique spectral signatures. Although the spectral response patterns of vegetation tend to be generally the same, small variations can be detected between and within vegetation types (because of their phenology, growth and vigour, crown pattern, association, and various other ecological parameters) and can therefore be studied using multi-spectral satellite images (Kachhwaha & sensing 1983).

Monitoring and characterising spatial patterns of Land-use/cover change is vital for understanding and predicting those changes (Petit *et al.* 2001), however, unlike land cover, land use typically must be inferred through a combination of remote-sensing observation, regional and local knowledge (including field observation), and other ancillary information that links a given land cover in a region with a given land use (Sohl *et al.* 2012).

Besides this, RS can also map and monitor changes in surface conditions, which are not related to a direct change in land cover or land use, most notably that of vegetation condition. Long term datasets such as those provided by the Landsat sensor since the 70s are particularly valuable for monitoring and understanding changes in vegetation condition (Wallace *et al.* 2006; Vogelmann *et al.* 2009).

Recent studies of land use changes caused by nuclear accidents were made following the Fukushima Daiichi nuclear disaster where RS was the only method by which these environmental changes could be analysed, since the area is set as an evaluation zone and direct monitoring is extremely difficult (Sekizawa *et al.* 2015).

1.7 Objectives

The objective of this work was to understand the main changes in the different land uses inside the CEZ. For this, analyses were made resorting to: Remote sensing techniques (OBIA – object-based Image Analyses); Satellite Images publicly available (Landsat); and Field training data collected in 2017. To determine trends over time of the sets of

classifications of land use the non-parametric Mann-kendall test and Sen's slope method were used.

2. Materials and Methods

2.1 Area of study

The Chernobyl Exclusion zone (CEZ) covers a radius of 30 km from the explosion site from which almost 2/3 of the total area are covered by forests (dominated by Scots pine) and grasslands, with the remaining area being mostly agricultural land around 1986 (Yoschenko *et al.* 2006; Hao *et al.* 2008; Banaszkiewicz *et al.* 2017).

The most visible effect of irradiation is seen in forest trees that grew in the nearest vicinity from the reactor (within 10 km) and where, in 1986, trees received the lethal dose (mainly from iodum), as shown in Figure 4. Nowadays, this forest is called the "red forest" (Tulik & Rusin 2005), although radiation is lower and trees are growing.

The trees that can be seen in Figure 5 are dead because they grew in a very wet area.



Figure 5 – Irradiated and damaged forest stands so-called “red forest” located within the territory of the 10-km zone around the Chernobyl nuclear power plant. The picture was taken in October 1997 by W. Wloch. (By Tulik & Rusin 2005, accessed: April 2023).

The area is no longer cultivated and due to land abandonment, no active forest and lack of fire management (because the forest was contaminated by radionuclides thus having limited commercial use), the vegetation overgrew. (Yoschenko *et al.* 2006; Hao *et al.* 2008).

Around 2016-2019 the status of the area changed and until the recent Russian invasion it was a touristic region. People began re-visiting the region for a variety of reasons. From displaced people (looking for a place to live); to scientists conducting studies of the effects of contamination on fauna and flora (Banaszkiewicz *et al.* 2017).

2.2 Fieldwork and Image Treatment

In October 2017, our team studied the Chernobyl Exclusion Zone with the objective of relating radiation with types of vegetation over time. More than 300 sites (that varied from points to lines and areas, were registered (using a Trimble Geo Explorer GPS device) along with the corresponding vegetation occupying the site.

Buffers were then added, in QGIS, between 1 and 5 meters to the lines and 20-meter buffers to the points that were later merged into a single shapefile (also containing the areas features retrieved during the field trip). He later downloaded the Landsat images (free satellite images) of the series 4, 5, 7 and 8, of the region from the Earth Explorer website from the United States Geographical Survey (USGS) which were subsequently treated for cloud contamination since clouds, along with their shadows cause significant problems for many remote sensing activities among which land cover classification and false detection of land cover change. For this, the cloud masking plugin – Bitbucket v18.2.7 – was used for QGIS as this plugin uses the Fmask algorithm which finds clouds and their shadows screening them effectively (Zhu & Woodcock 2012). To obtain an accurate cloud mask for each image the values for the cloud probability threshold of the Fmask algorithm were adjusted, and in order to complete the cloud masking, through manual processing using R software, the cloud mask layer cropped the stacked image an then a reclassification of pixels was performed (Santos *et al.* 2019b).

I, in the beginning of this project, revised all the images as well as every process they underwent to minimise the margin for error. In addition, a new search of images was conducted but no better images were found besides the ones already downloaded in 2017.

2.3 Images Classification

As described by Kerle *et al.* (2004), image classification follows a very simple principle: a pixel is assigned to a class based on its feature vector through comparison of predefined clusters (classes) in the feature space. The clusters can either be defined automatically via an Unsupervised image classification, where a clustering algorithm finds and defines several clusters in the feature space or, through a Supervised image classification in which case the area of interest needs to be known by the operator through previous experience or through field data collected in the past.

Because I had access to the images and data collected in 2017, I resorted to Supervised Image Classification. As training areas (sample areas) I used all the 300 recorded sites as training areas (sample area).

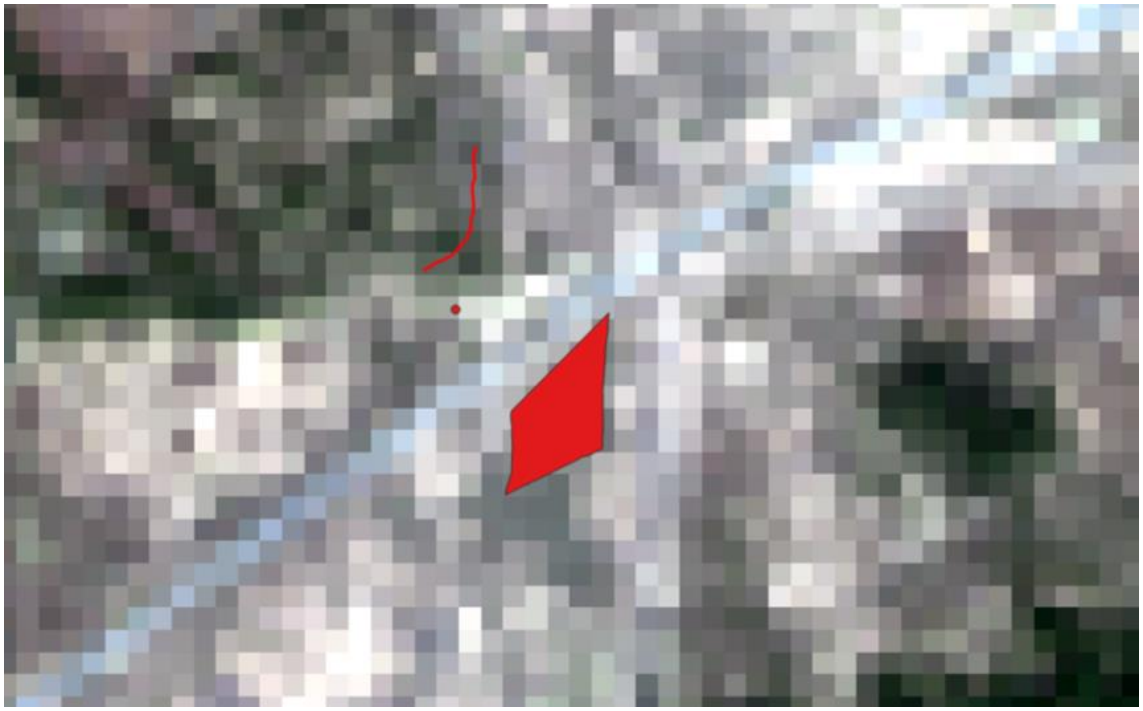


Figure 6 – Close-up of 3 sampled locations(red) inside the 30 km CEZ from the year 2017.



Figure 7 – Landsat satellite image from Chornobyl Nuclear Power Plant from the year 1984, contaminated with clouds.

Although images from 1984 to 2017 were downloaded, not all were used. Starting from the year of the accident, several years were selected with a 5-year interval between them (as this interval would be enough to demonstrate land use changes and would ensure a longer temporal interval for the study), and two images were taken from each year.

Images from years prior to the accident were either too clouded even after being treated with cloud masking (as shown in figure 5) or non-existent and therefore could not be used. This problem did not happen in years that followed the accident although some degree of contamination was inevitable and would later interfere with some results. The year of the accident was the only one that presented a single viable image (taken in spring).

I used the Semi-Automatic Classification Plugin (SCP), developed by Luca Congedo (Congedo 2016), in QGIS to classify the images and began by the year 2017 as that was the year that I possessed training data on. The bands from the Landsat used for the classification were bands from B1 up to B7. After that, I started analysing and classifying the years prior to 2017 using visual interpretation of the satellite images in accordance with the training data from the field trip.

The names of the sample sites were given in accordance with the types of vegetation classes that they contained, but because most contained several vegetation types classes were rearranged as shown in table 1.

Table 1 – List of vegetation classes analysed and their description.

Vegetation Classes	Description
Pines	Homogeneous patch of *Pines*
Grassland	Homogeneous patch of Grassland
Betula	Homogeneous patch of *Betula*
Alder	Homogeneous patch of *Alder*
Oaks	Homogeneous patch of *Oaks*
Robinia pseudoacacia	Homogeneous patch of *Robinia pseudoacacia*
Marshland	Homogeneous patch of Marshland
Robinia	Homogeneous patch of *Robinia*

Field	Patch of agricultural land
Mixed	Heterogeneous patch where there is not any dominant vegetation
Grassland Trees	Heterogeneous patch where grassland is dominant
Deciduous Forest	Heterogeneous patch of Deciduous trees
Water	The Chernobyl cooling pound, Prypiat river and other small lakes and ponds spread through the CEZ
Sand	Patch of sand

Even though some classes, such as *Robinia pseudoacacia*, Marshlands, and *Robinia*, presented a low number of pixels, they were not omitted from the classification and testing procedures as they are essential vegetation classes.

The classified images were then divided into 2 datasets based on the date they were taken, the Foliage dataset (images dating from May 1st to September 15th) and the No-Foliage dataset (images dating from September 16th to April 30th).

2.3.1 The Minimum Distance Method

For the image classification, I used the Minimum Distance Method, in which the Euclidean distances from an unknown pixel to various cluster centers are calculated. For each pixel, the measurements of its EM energy value are stored as a Digital Numbers or DN-value. Once the classification starts, each pixel in the image is assigned to one of the predefined classes, to which the distance to the mean DN-value is least, based on its own DN-value (Kerle *et al.* 2004). Through this method, it is possible to simultaneously classify all classes (Wacker & Landgrebe 1972). A colour was then added to each class so that, in the final product, the pixels corresponding to said class would be coloured by the corresponding colour. This would facilitate, not only to see the regions where each class was more prevalent but also to understand how the classes evolved throughout the years.

2.3.2 Validation of the classification maps

Accuracy assessment is a fundamental step after land cover classification in order to evaluate errors, globally and for each class, and finally evaluate the reliability of the map (Congedo 2016). The “Accuracy” tool in SCP accomplishes this task, providing the error matrix, the Kappa-value (a statistic used to measure inter-rater reliability for qualitative items) and the accuracy estimates (Byrt *et al.* 1993; Xia & Science 2020).

2.4 Temporal Analyses

As stated by Hussain and Mahmud (2019), trend analysis is one of the most important measurements in studying time series data. One of the most used non-parametric trend tests to assess the significance of trends in time series is the Mann-Kendall test (Hamed & Rao 1998; Gocic *et al.* 2013). Therefore, the non-parametric Mann-Kendall and Sen's methods were used to determine whether there was a positive, negative, or neutral trend. For a better understanding of the results, a Sen’s slope graphic was generated for each individual class. The p-value (two tailed), along with the standard deviation and Mean of each class, were also calculated to better understand how they varied from one another. These tests were conducted using RStudio, and the graphics were generated with XLSTAT (a tool for statistical analyses).

3. Results

3.1 Classification

The classification of each map was the first visual representation obtained of the evolution of the different vegetation classes throughout the years. When comparing the first maps of each season (1986 Foliage and the No Foliage 1990) with the last classified maps (Foliage 2017 and No Foliage 2017) the most dominant trend is the diminishing of the Field class (purple pixels).

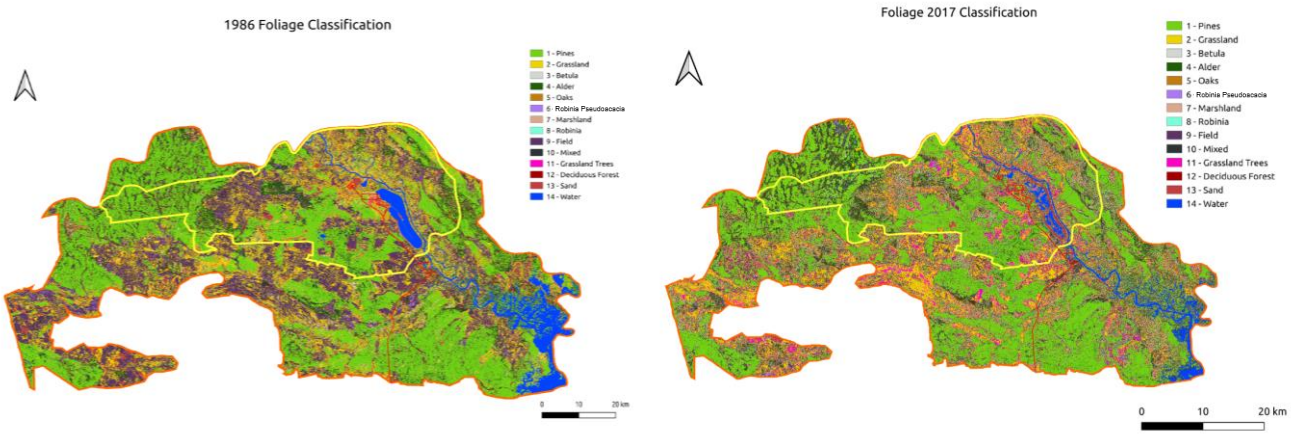


Figure 8 - 1986 and 2017 Foliage Season classification maps

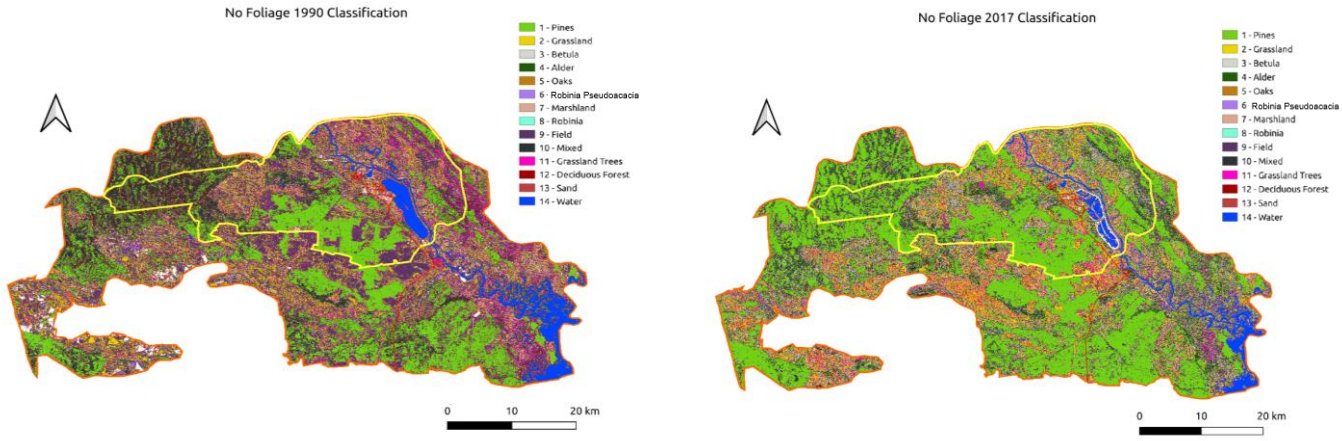


Figure 9 - 1990 and 2017 No Foliage Season classification maps

Appendices I and II at the end of this document provide all the images of the classifications of each year from both datasets.

3.2 Global Trends

Both the Fields and Grassland classes present a prominent trend: over time, the number of pixels in the Fields class decreases while the number of pixels in the Grassland class increases. (Figures 10 and 11, which show the Foliage and No-Foliage periods, respectively). In addition to this, the number of pixels of Betula, Oak, Robinia pseudoacacia, Mixed and Grassland Trees classes also rose while remaining unchanged for Pines, Alder, Marshland, Robina, and Deciduous Forest. The only class in both datasets that decreased over time was the Field class.

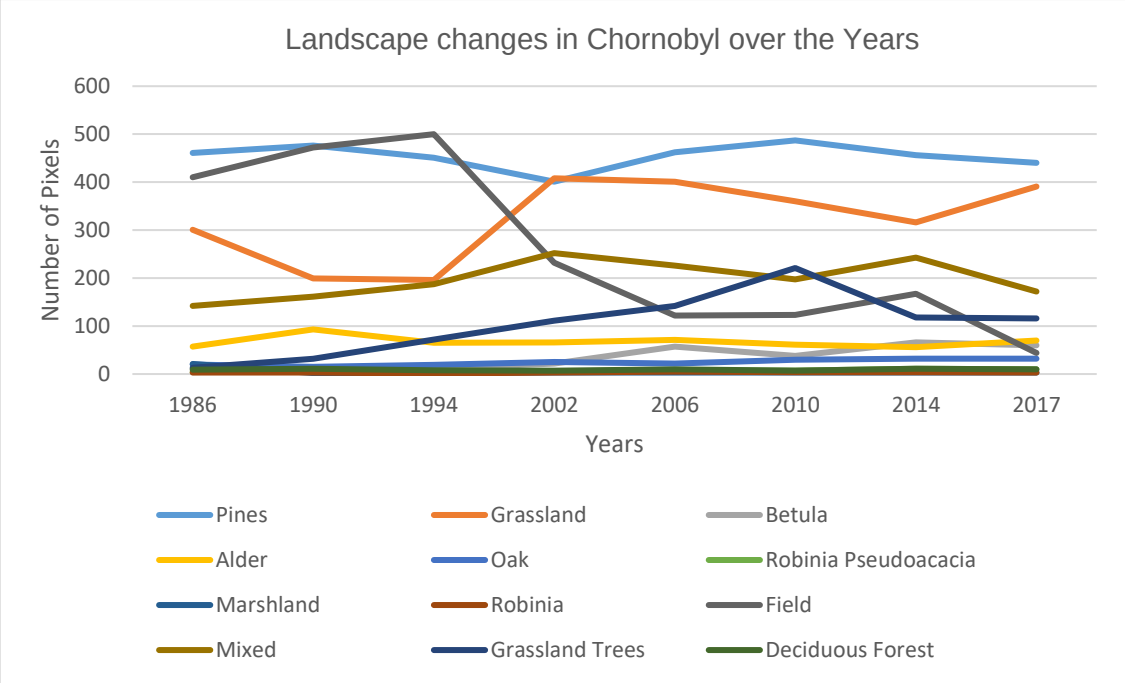


Figure 10 - Progression of the landscape change in Chornobyl over the course of a year during the Foliage phase. The y-axis represents the number of pixels in the classified photographs and how they evolved throughout the years.

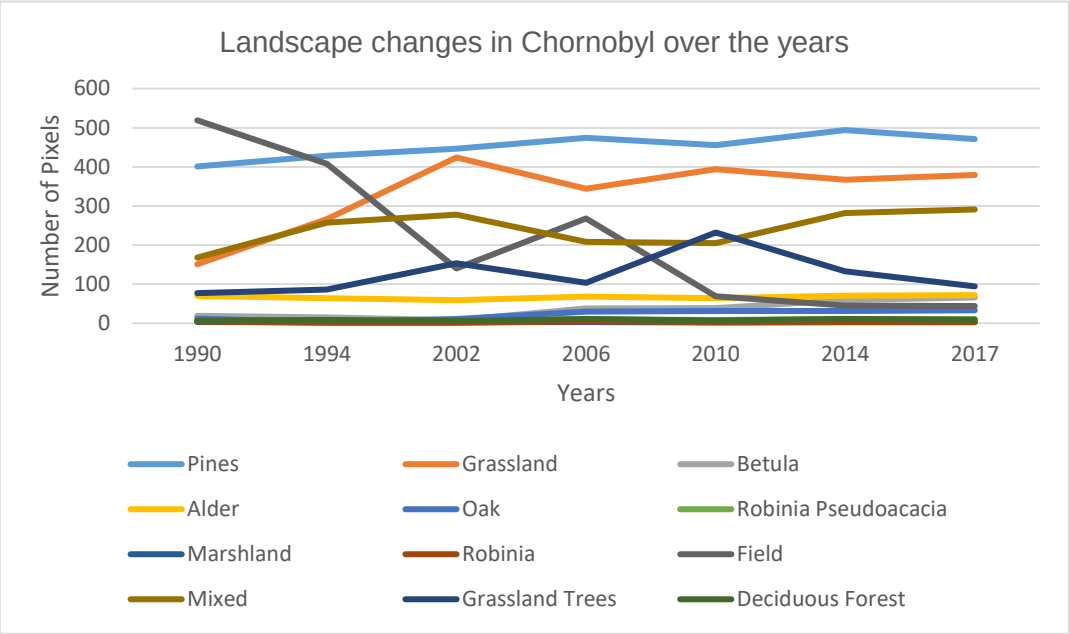


Figure 11 - Progression of the landscape change in Chornobyl over the course of a year during the No-Foliage phase. The y-axis represents the number of pixels in the classified photographs and how they evolved throughout the years. Although both graphs' y-axes terminate in 2017 (the year the information was obtained), the graphic from the No-Foliage period begins in 1990 since there were no suitable photos from the year of the accident.

The vegetation class from the Foliage dataset with the lowest mean is Robinia (3.250 pixels per image; Table 2). This class also has the lowest standard deviation (1.165). However, in the case of the No-Foliage dataset, both Robinia and Marshland classes have the same mean value, which is the lowest of all classes (2.857; Table 3). The Marshland class also has the lowest standard deviation in this dataset (0.378; Table 3). In both datasets, the Pines vegetation class has the highest mean, with 454,250 and 452,714, respectively (Tables 2 and 3).

Table 2 - Summary Statistics Table for the Foliage dataset. The observations column represents the number of images that were classified.

Variable	Observations	Minimum	Maximum	Mean	Std. deviation
Pines	8	401,000	487,000	454,250	25,922
Grassland	8	196,000	408,000	321,500	85,625
Betula	8	11,000	66,000	34,625	23,688
Alder	8	56,000	93,000	67,375	11,722
Oak	8	15,000	32,000	24,375	6,435
Robinia Pseudoacacia	8	4,000	11,000	7,250	2,375
Marshland	8	2,000	21,000	5,000	6,481
Robinia	8	1,000	5,000	3,250	1,165
Field	8	44,000	500,000	258,750	176,851
Mixed	8	142,000	252,000	197,500	39,688
Grassland Trees	8	13,000	221,000	103,125	65,471
Deciduous Forest	8	7,000	11,000	9,125	1,642

Table 3 - Summary Statistics Table for the No Foliage dataset. The observations column represents the number of images that were classified.

Variable	Observations	Minimum	Maximum	Mean	Std. deviation
Pines	7	401,000	494,000	452,714	31,165
Grassland	7	151,000	424,000	332,143	93,988
Betula	7	8,000	66,000	34,857	22,162
Alder	7	59,000	72,000	66,857	4,706
Oak	7	3,000	33,000	21,571	12,435
Robinia Pseudoacacia	7	4,000	11,000	8,143	2,673
Marshland	7	2,000	3,000	2,857	0,378
Robinia	7	1,000	5,000	2,857	1,464
Field	7	44,000	519,000	213,286	190,410
Mixed	7	168,000	291,000	241,286	47,468
Grassland Trees	7	77,000	232,000	125,429	54,107
Deciduous Forest	7	6,000	11,000	8,286	1,976

There were no differences between the types of vegetation in the two seasons (ANOVA test, Table 4).

Table 4 - Results of the ANOVA Test. SS - Sum of Squares - quantifies the variability between or within the groups; df - degrees of freedom; MS - Mean Square - average variation either between or within the groups; F - statistical test used in one-way ANOVA; P-value indicates whether to accept the null hypothesis or the alternative hypothesis; F critical value indicates if the test is significant

Source of Variation	*SS*	*df*	*MS*	*F*	*P-value*	*F critical*
Between Groups	24,3009375	1	24,3009375	0,00106993	0,974200979	4,300949502
Within Groups	499678,3473	22	22712,65215			
Total	499702,6482	23				

3.3 Local Trends

Marshland was the only class that presented a Sen's slope value of 0.000 (therefore, no trend) in both datasets (Tables 4 and 5). Robinia also exhibits a Sen's Slope value of 0.000 in the No-Foliage class; however, in the Foliage table, it presents an increasing slope (0,018). Only two classes in the Foliage dataset had a decreasing slope: Alder (-

0,063) and Pines (-0,578). The Field class is the only one that presents a decreasing slope in both datasets (-12,621 and -17,593 in the Foliage and No-Foliage datasets, respectively).

Table 5 - Results of the Mann-Kendall and p-value tests and Sen´s Slope value of the Foliage dataset. The Sen's Slope values indicate the type of trend. Positive numbers indicate positive trends; negative values indicate negative trends; and zero indicates no trend (neutral).

Series\Test	Kendall's tau	p-value	Sen's slope
Pines	-0,143	0,711	-0,578
Grassland	0,214	0,536	3,666
Betula	0,837	**0,006**	1,720
Alder	-0,071	0,902	-0,063
Oak	0,764	**0,013**	0,533
Robinia Pseudoacacia	0,691	**0,025**	0,174
Marshland	0,138	0,772	0,000
Robinia	0,289	0,421	0,018
Field	-0,571	0,063	-12,621
Mixed	0,357	0,266	2,208
Grassland Trees	0,643	**0,035**	4,813
Deciduous Forest	0,038	1,000	0,000

Table 6 - Results of the Mann-Kendall and p-value tests and Sen´s Slope value of the No Foliage dataset. The Sen's Slope values indicate the type of trend. Positive numbers indicate positive trends; negative values indicate negative trends; and zero indicates no trend (neutral).

Series\Test	Kendall's tau	p-value	Sen's slope
Pines	0,714	**0,035**	2,593
Grassland	0,429	0,230	5,050
Betula	0,714	**0,035**	2,200
Alder	0,390	0,288	0,333
Oak	0,781	**0,023**	0,950
Robinia Pseudoacacia	0,683	**0,048**	0,250
Marshland	-0,178	0,803	0,000
Robinia	0,053	1,000	0,000
Field	-0,905	**0,007**	-17,593
Mixed	0,524	0,133	2,500
Grassland Trees	0,333	0,368	1,625
Deciduous Forest	0,309	0,437	0,125

The Sen's Slopes graphics (figures 12, 13, 14, and 15), produced by the Mann-Kendall test provided us with a graphical representation of the evolution of the number of pixels of each class throughout the years until 2017.

The two most significant trends are the significant decrease in pixel number of the Field class, which in 1986 in the Foliage dataset presented 410 pixels and in 2017 was only composed of 44 pixels, and the increase, also in the Foliage dataset, in the Grassland

class, which went from 301 pixels in 1986 to 391 pixels in 2017. Similarly, in the No-Foliage dataset, the same occurred as the decrease in the number of pixels in the Field class went from 519 to 44 and the increase in the Grassland class went from 151 to 379 pixels.

Other classes also presented changes throughout the years, but the most prominent ones, in both seasons, were from the Fields and Grassland classes. It is, however, worth noting that the Grassland Trees class, similarly to the Grassland class, also presented a big increase throughout the years (from 13 pixels in 1986 to 116 in 2017 in the Foliage dataset, and from 77 pixels in 1986 passing through 232 in 2010 and presenting a final reading of 94 pixels in 2017 in the No Foliage dataset).

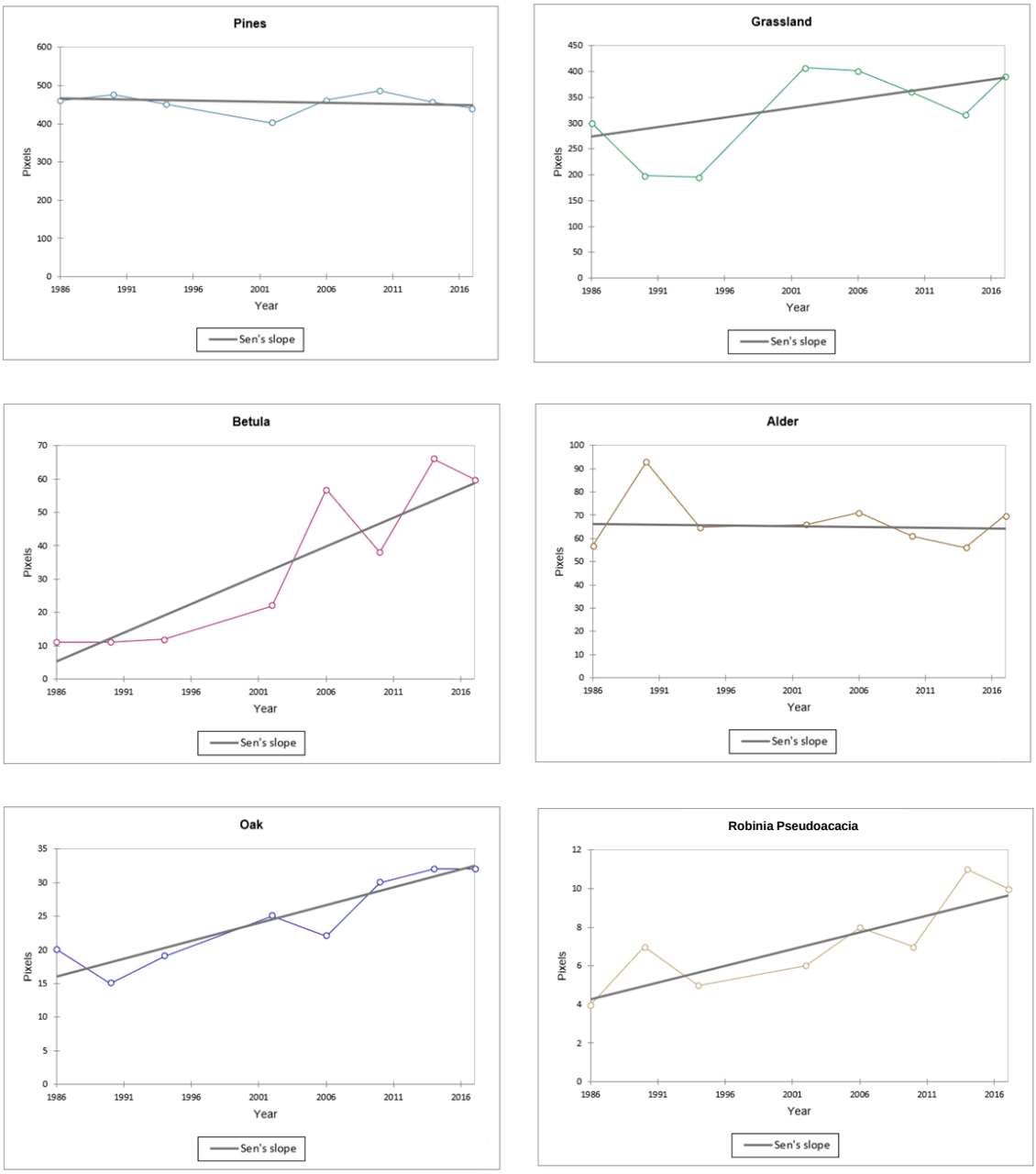


Figure 12 - Foliage dataset Sen's Slopes of the Pines, Grassland, Betula, Alder, Oak and Robinia Pseudoacacia classes

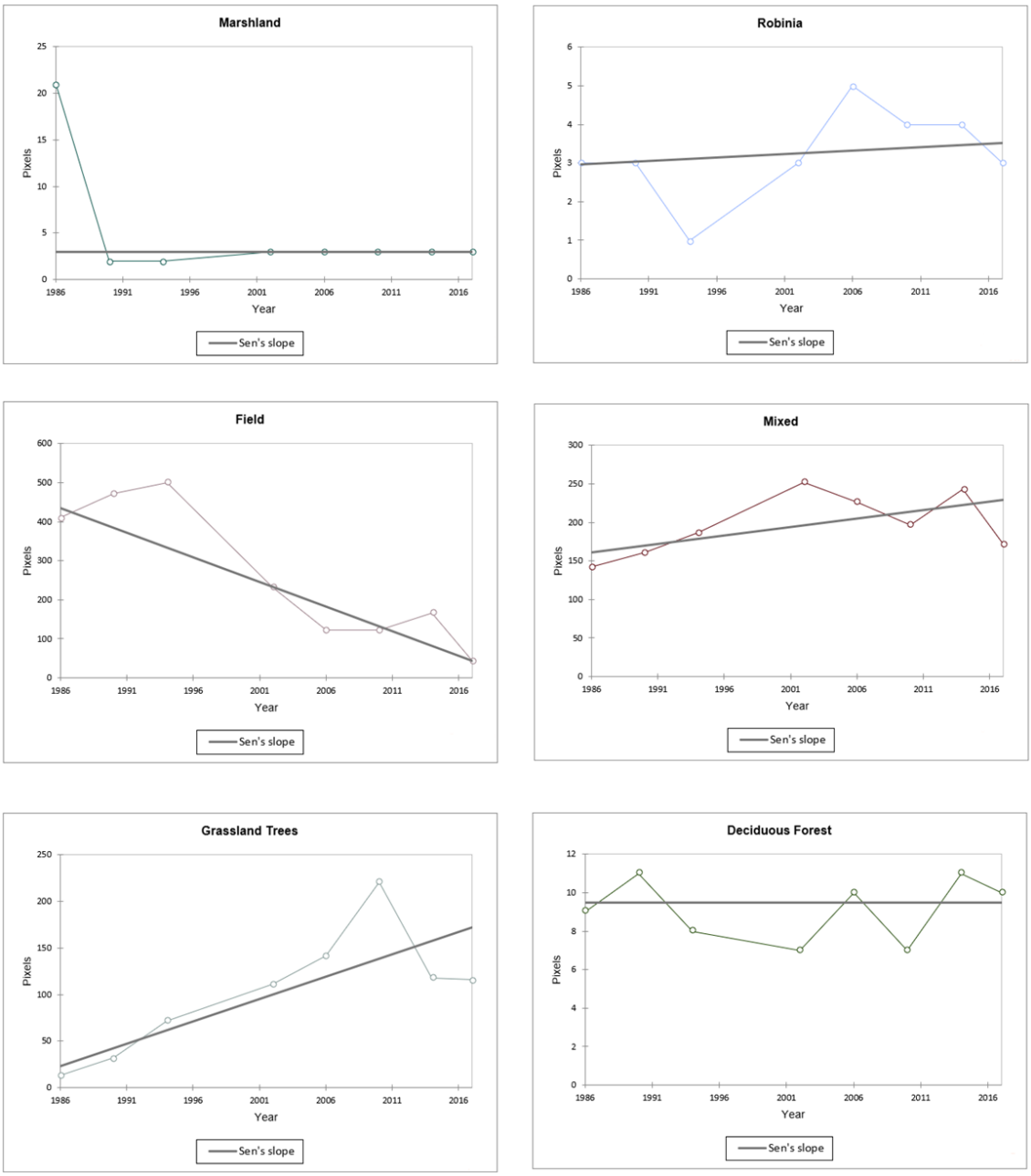


Figure 13 - Foliage dataset Sen's Slopes of the Marshland, Robinia, Field, Mixed, Grassland Trees and Deciduous Forest classes

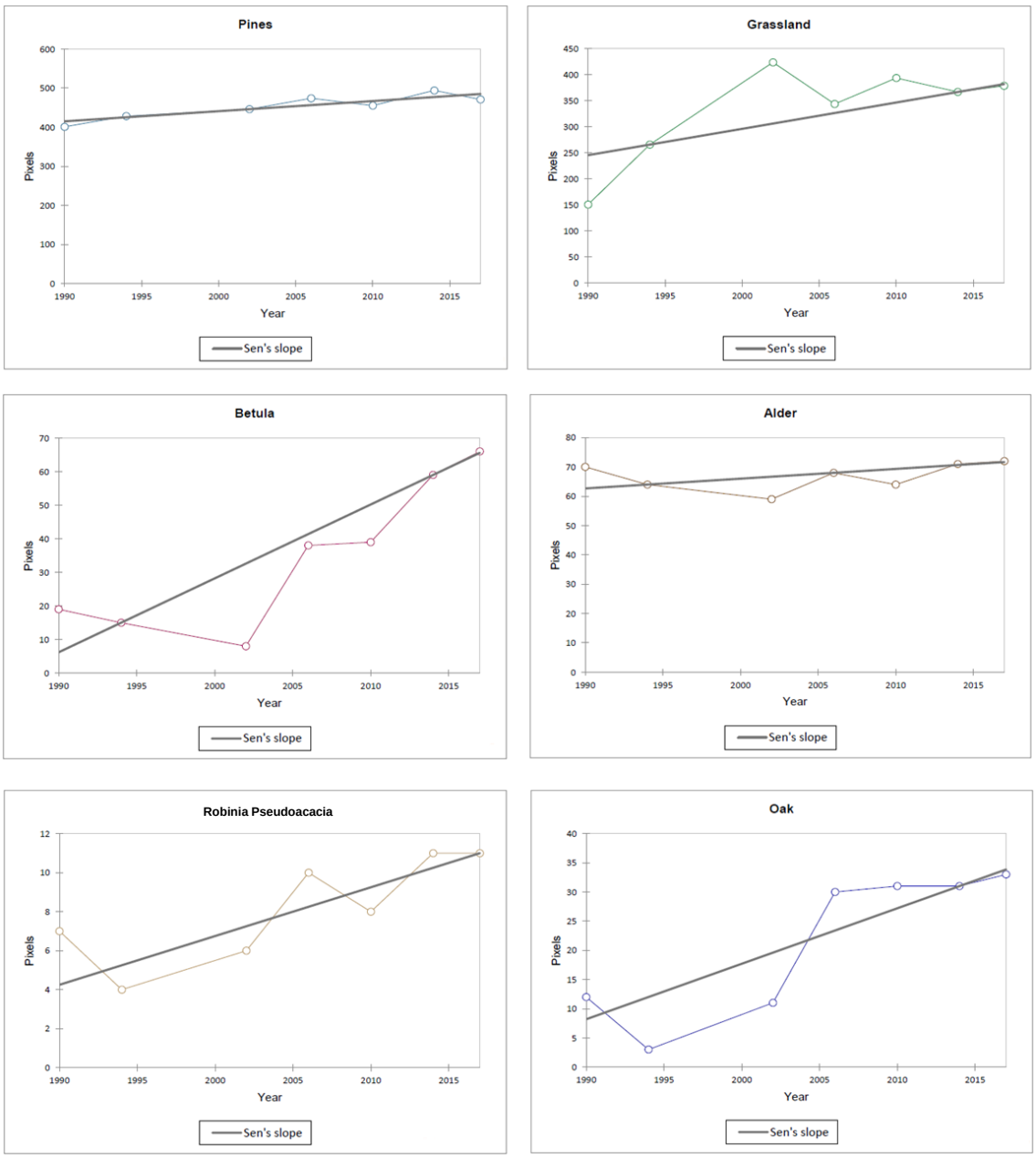


Figure 14 - No Foliage dataset Sen's Slopes of the Pines, Grassland, Betula, Alder, Oak and Robinia Pseudoacacia classes

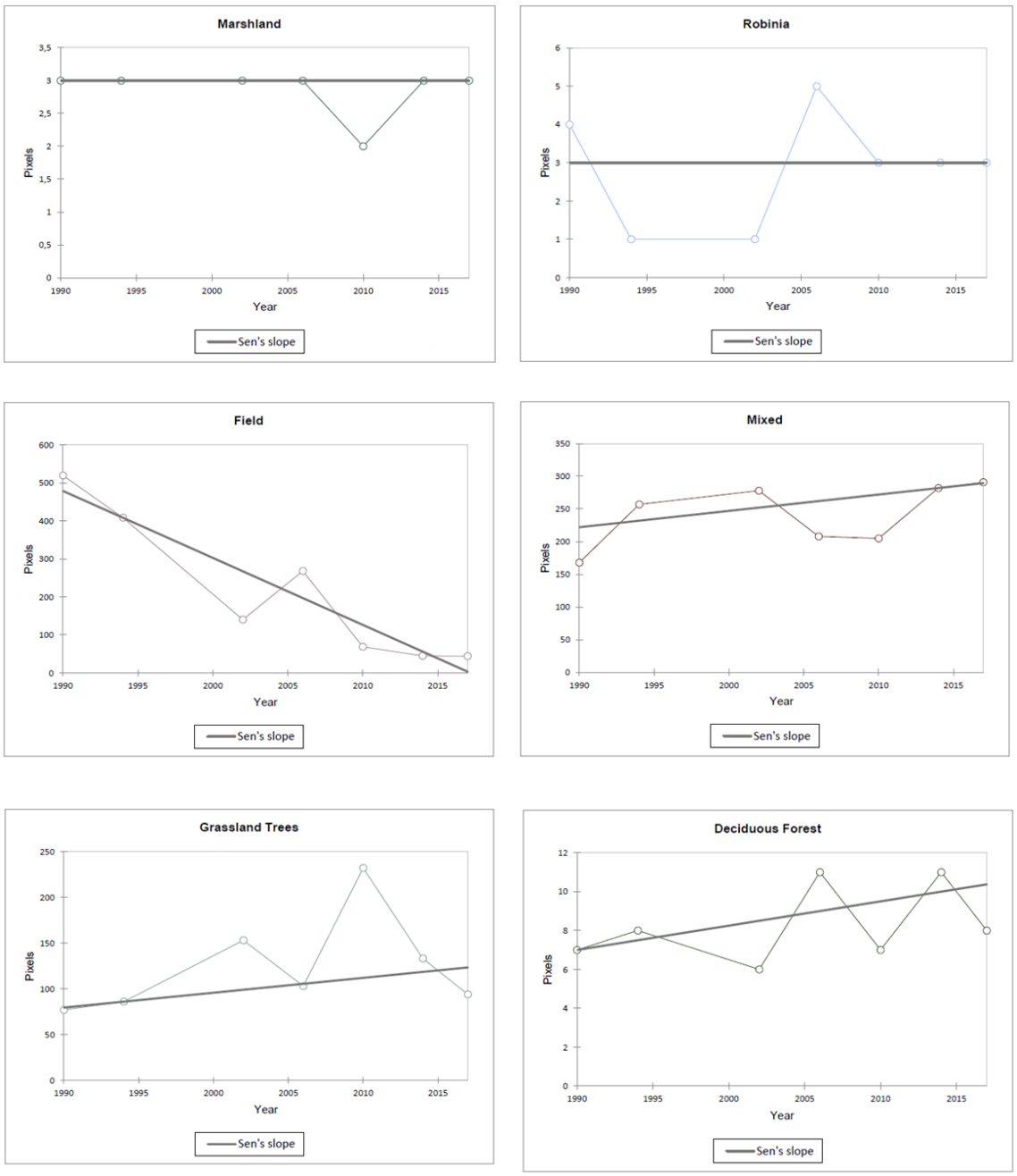


Figure 15 - No Foliage dataset Sen's Slopes of the Marshland, Robinia, Field, Mixed, Grassland Trees and Deciduous Forest classes

4. Discussion

Classifications of the 30-kilometer CEZ revealed noticeable changes throughout the years, with one noteworthy shift being the pronounced diminishing in the number of pixels in the Field class. Additionally, during the Foliage season, both the Pines and Alder classes saw a small decline in their pixel numbers; however, it is important to note that this reduction was not equivalent to the changes seen in the Field class, and both the Pines and Alder classes presented increasing trends in their pixel numbers on the No-Foliage season. All other classes, in both seasons, showed an increase in pixel numbers, with the Grassland class having the most prominent one out of any other class and occupying all fields. The apparent diminishing in water availability over the years could be explained by several reasons; in some years it may not have rained as much as in others, which directly affects the amount of water available. Another reason could be that vegetation started to occupy the margins of the river as the years passed which led to a decrease in the water pixels in the classifications.

The Sen's Slopes acquired using the Mann-Kendall test offered additional support to this result, illustrating in greater detail the evolution of each individual class throughout the years. These results point to an improvement in the vegetation over the years after the accident, following the land abandonment of the population. The high capacity of the forest when serving as a biogeochemical barrier and the relatively slow migration of strontium and caesium radionuclides along the forest soil profile allied with the positive effects of land abandonment and reduced abundance of herbivores explain the natural ecological succession observed and the increase in green coverage in the exclusion zone and current, seemingly unaffected flora by the radiation effects (Tikhomirov & Shcheglov ; Shcheglov *et al.* ; Mousseau & Moller 2020).

In their study, Krouglov *et al.* (1997), observed that the ^{137}Cs soil-to-plant concentration ratios, initially showed values that were at first elevated but reduced more than 50 times in the following years, which was attributed to the fixation of radionuclides by soil mineral fraction, that prevented further uptake by plants. These findings align with the results of our study that demonstrate a gradual improvement in vegetation over the years following the accident indicating that the positive effect of land abandonment is greater than the negative effect caused by low levels of radiation exposure on the vegetation (Davydchuk 1997; Santos *et al.* 2019; Gemitzi 2020).

Other works also demonstrated that the ecological status of the Scot pine trees can be fully restored during 30-40 years after acute exposure to radiation (Holiaka *et al.* 2020).

The effects of the operations to clean the ground may also have reduced radiation exposure to a level that vegetation can tolerate and still grow without major reductions in fitness; however, because the deposition of radionuclides was highly heterogeneous the levels of ionising radiation varied within short distances making the evolution of vegetation across the region differ inside the CEZ even after the cleaning operations (Ipatyev *et al.*; Fesenko *et al.*; Boratyński *et al.* 2016).

Caution is urged while analysing the results obtained from the Mann-Kendall test since few were significant, which were prompted by the following limitations of the present work: Firstly, not all satellite images could be used for the classification process, as some were highly contaminated by clouds. Although this didn't affect the Mann-Kendall test, it did limit our dataset to only one image prior to the accident (1986 Foliage), which reduced my understanding of the original populations under study. Even among the images that were used, despite undergoing cloud masking treatment, some contamination was unavoidable. This residual cloud contamination ultimately affected the results significantly impeding the accuracy and reliability of the classification process.

Another aspect that led to these results was the classification method used. As expressed in Kerle *et al. (2004)*, the Minimum Distance to Mean (MDM) classifier presents some disadvantages compared to other classification methods, such as pixels being assigned to the cluster center closer to them (which may not always be the proper cluster). Furthermore, MDM ignores class variability (some clusters are small and dense, while others are large and dispersed), whereas Maximum Likelihood classification does. Despite this, it was the only test that could be used due to a programming bug which led to unsatisfactory results from the other tests (Maximum Likelihood, SAM, and Random Forest).

The lack of statistical significance in the results can be attributed to several factors, with one key factor being the in-situ data collected during the field trip (Beaugelin-Seiller *et al.* 2020). Some of the training data points gathered were insufficient in quantity to adequately represent certain classes. For instance, when considering the Marshland class, only three training points were collected, which significantly reduced its representation within the dataset, however, while this lack of representation could be

attributed to the limited number of data points it is important to understand that classes may naturally occur at different frequencies and the infrequency of a class, such as the Marshland class is not inherently a problem but rather a characteristic of the studied environment.

5. Conclusion

Although it is known that chronic radiation, among other effects, damages genetic material and can be lethal at high doses (Dowlath *et al.* 2021), the results of this study show that due to a gradual reduction of the radiation levels and the land abandonment (result of the evacuation that followed the accident), natural regeneration and ecological succession can be observed.

It is clear that throughout the years, the once agricultural fields inside the CEZ have started to be populated by a mix of different types of vegetation and transformed into a more heterogeneous landscape.

Further studies should be conducted with different and better methods of classification to better understand the land use changes and how the vegetation adapted throughout the years with a greater degree of confidence. A proper control region with a similar level of land abandonment but less contamination will help to distinguish the effects of chronic ionizing radiation from direct human land use influences.

References

1. Aguileta, G., Badouin, H., Hood, M.E., Møller, A.P., Le Prieur, S., Snirc, A. *et al.* (2016). Lower prevalence but similar fitness in a parasitic fungus at higher radiation levels near Chernobyl. 25, 3370-3383.

2. Akbari, H., Rose, L.S., Taha, H.J.L. & planning, u. (2003). Analyzing the land cover of an urban environment using high-resolution orthophotos. 63, 1-14.

3. Aktipis, C.A., Boddy, A.M., Jansen, G., Hibner, U., Hochberg, M.E., Maley, C.C. *et al.* (2015). Cancer across the tree of life: cooperation and cheating in multicellularity. 370, 20140219.

4. Banaszkiewicz, M., Kruczek, Z. & Duda, A.J.F.T.A.W.F.i.B.C.w.K. (2017). The Chernobyl exclusion zone as a tourist attraction: Reflections on the turistification of the zone. 145-169.

5. Beaugelin-Seiller, K., Garnier-Laplace, J. & Beresford, N.A.J.J.o.e.r. (2020). Estimating radiological exposure of wildlife in the field. 211, 105830.

6. Beresford, N.A., Scott, E.M. & Copplestone, D.J.J.o.E.R. (2020). Field effects studies in the Chernobyl Exclusion Zone: Lessons to be learnt. 211, 105893.

7. Bonisoli-Alquati, A., Voris, A., Mousseau, T.A., Møller, A.P., Saino, N., Wyatt, M.D.J.C.B. *et al.* (2010). DNA damage in barn swallows (Hirundo rustica) from the Chernobyl region detected by use of the comet assay. 151, 271-277.

8. Boratyński, Z., Arias, J.M., Garcia, C., Mappes, T., Mousseau, T.A., Møller, A.P. *et al.* (2016). Ionizing radiation from Chernobyl affects development of wild carrot plants. 6, 39282.

9. Byrt, T., Bishop, J. & Carlin, J.B.J.J.o.c.e. (1993). Bias, prevalence and kappa. 46, 423-429.

10. Caplin, N. & Willey, N. (2018a). Ionizing Radiation, Higher Plants, and Radioprotection: From Acute High Doses to Chronic Low Doses. *Front Plant Sci*, 9, 847.

11. Caplin, N. & Willey, N.J.F.i.p.s. (2018b). Ionizing radiation, higher plants, and radioprotection: from acute high doses to chronic low doses. 9, 847.

12. Carlson, T. & Sanchez-Azofeifa, G.A.J.R.S.o.E. (1999). Satellite remote sensing of land use changes in and around San Jose, Costa Rica. 70, 247-256.

13. Congedo, L.J.R. (2016). Semi-automatic classification plugin documentation. 4, 29.

14. de Empresas Petrolíferas, A.P. (2016). Guia Setorial para a Proteção e Remediação de Solos e Águas Subterrâneas no Setor Petrolífero. Apetro.

15. Davydchuk, V.J.E.E. (1997). Ecosystem remediation in radioactively polluted areas: the Chernobyl experience. 8, 325-336.

16. De Ruysscher, D., Niedermann, G., Burnet, N.G., Silva, S., Lee, A.W. & Hegi-Johnson, F. J. N. R. D. P. (2019). Radiotherapy toxicity.5, 13.

17. Dighton, J., Tugay, T. & Zhdanova, N. (2008). Fungi and ionizing radiation from radionuclides. *FEMS Microbiology Letters*, 281, 109-120.

18. Dowlath, M.J.H., Karuppannan, S.K., Sinha, P., Dowlath, N.S., Arunachalam, K.D., Ravindran, B. *et al.* (2021). Effects of radiation and role of plants in radioprotection: A critical review. 779, 146431.

19. Esnault, M.-A., Legue, F., Chenal, C.J.E. & Botany, E. (2010). Ionizing radiation: advances in plant response. 68, 231-237.

20. Fesenko, S., Jacob, P., Ulanovsky, A., Chupov, A., Bogdevich, I., Sanzharova, N. *et al.* (2013). Justification of remediation strategies in the long term after the Chernobyl accident. 119, 39-47.

21. Filburn, T., Bullard, S. & Bullard, S.G. (2016). *Three Mile Island, Chernobyl and Fukushima*. Springer.

22. Foray, N., Bourguignon, M. & Hamada, N.J.M.R.R.i.M.R. (2016). Individual response to ionizing radiation. 770, 369-386.

23. Franklin, J., Woodcock, C., Warbington, R.J.P.E. & Sensing, R. (2000). Digital vegetation maps of forest lands in California: integrating satellite imagery, GIS modeling, and field data in support of resource management. 66, 1209-1217.

24. Garnier-Laplace, J., Geras'kin, S., Della-Vedova, C., Beaugelin-Seiller, K., Hinton, T., Real, A. *et al.* (2013). Are radiosensitivity data derived from natural field conditions consistent with data from controlled exposures? A case study of Chernobyl wildlife chronically exposed to low dose rates. 121, 12-21.

25. Gemitzi, A.J.L. (2020). Are vegetation dynamics impacted from a nuclear disaster? The case of Chernobyl using remotely sensed NDVI and land cover data. 9, 433.

26. Gocic, M., Trajkovic, S.J.G. & Change, P. (2013). Analysis of changes in meteorological variables using Mann-Kendall and Sen's slope estimator statistical tests in Serbia. 100, 172-182.

27. Hamed, K.H. & Rao, A.R.J.J.o.h. (1998). A modified Mann-Kendall trend test for autocorrelated data. 204, 182-196.

28. Hao, W.M., Bondarenko, O.O., Zibtsev, S. & Hutton, D.J.D.i.e.s. (2008). Vegetation fires, smoke emissions, and dispersion of radionuclides in the Chernobyl exclusion zone. 8, 265-275.

29. Hatch, M., Ron, E., Bouville, A., Zablotska, L. & Howe, G.J.E.r. (2005). The Chernobyl disaster: cancer following the accident at the Chernobyl nuclear power plant. 27, 56-66.

30. Hinton, T.G., Alexakhin, R., Balonov, M., Gentner, N., Hendry, J., Prister, B. *et al.* (2007). RADIATION-INDUCED EFFECTS ON PLANTS AND ANIMALS: FINDINGS OF THE UNITED NATIONS CHERNOBYL FORUM. 93, 427-440.

31. Holiaka, D., Fesenko, S., Kashparov, V., Protsak, V., Levchuk, S. & Holiaka, M.J.J.o.e.r. (2020). Effects of radiation on radial growth of Scots pine in areas highly affected by the Chernobyl accident. 222, 106320.

32. Hussain, M. & Mahmud, I.J.J.o.O.S.S. (2019). pyMannKendall: a python package for non parametric Mann Kendall family of trend tests. 4, 1556.

33. Imanaka, T. (2002). *Recent Research Activities about the Chernobyl NPP Accident in Belarus, Ukraine and Russia*. Research Reactor Institute, Kyoto University.

34. Ipatyev, V., Bulavik, I., Baginsky, V., Goncharenko, G. & Dvornik, A.J.J.o.E.R. (1999). Forest and Chernobyl: forest ecosystems after the Chernobyl nuclear power plant accident: 1986–1994. 42, 9-38.

35. Jensen, J.R. (2009). *Remote sensing of the environment: An earth resource perspective 2/e*. Pearson Education India.

36. Josephson, P.R. (2005). *Red atom: Russia's nuclear power program from Stalin to today*. University of Pittsburgh Pre.

37. Kachhwaha, T.J.P.e. & sensing, r. (1983). Spectral signatures obtained from Landsat digital data for forest vegetation and land-use mapping in India. 49, 685-689.

38. Kerle, N., Janssen, L.L. & Huurneman, G.C.J.I., Educational textbook series (2004). Principles of remote sensing. 2, 250.

39. Kovalchuk, O., Dubrova, Y.E., Arkhipov, A., Hohn, B. & Kovalchuk, I.J.N. (2000). Wheat mutation rate after Chernobyl. 407, 583-584.

40. Krouglov, S., Filipas, A., Alexakhin, R. & Arkhipov, N.J.J.o.e.r. (1997). Long-term study on the transfer of 137Cs and 90Sr from Chernobyl-contaminated soils to grain crops. 34, 267-286.

41. L'Annunziata, M.F. (2007). Introduction: Radioactivity and our Well-Being. In: *Radioactivity: Introduction and History* (ed. Science, E) Netherlands, Amsterdam, pp. 1-45.

42. Lowe, D., Roy, L., Tabocchini, M.A., Rühm, W., Wakeford, R., Woloschak, G.E. *et al.* (2022). Radiation dose rate effects: what is new and what is needed? , 61, 507-543.

43. Ludovici, G.M., Oliveira de Souza, S., Chierici, A., Cascone, M.G., d'Errico, F. & Malizia, A. (2020). Adaptation to ionizing radiation of higher plants: From environmental radioactivity to chernobyl disaster. *J Environ Radioact*, 222, 106375.

44. Medvedev, G. (1989). JPRS Report, Soviet Union: Economic Affairs (" Chernobyl Notebook" By G. Medvedev, Published in Novy Mir, June 1989). JOINT PUBLICATIONS RESEARCH SERVICE ARLINGTON VA.

45. Mettler, F.A. & Upton, A.C. (2008). *Medical effects of ionizing radiation*. Saunders/Elsevier.

46. Møller, A.P. & Mousseau, T.A.J.B.R. (2013). The effects of natural variation in background radioactivity on humans, animals and other organisms. 88, 226-254.

47. Mousseau, T.A., Milinevsky, G., Kenney-Hunt, J. & Møller, A.P.J.O. (2014). Highly reduced mass loss rates and increased litter layer in radioactively contaminated areas. 175, 429-437.

48. Mousseau, T.A. & Moller, A.P. (2020). Plants in the Light of Ionizing Radiation: What Have We Learned From Chernobyl, Fukushima, and Other "Hot" Places? *Front Plant Sci*, 11, 552.

49. Mousseau, T.A.J.A.r.o.e., evolution, & systematics (2021). The biology of Chernobyl. 52, 87-109.

50. Murphy, B.D. (2006). *ORIGEN-ARP Cross-Section Libraries for the RBMK-1000 System*. UT-Batelle, LLC, Oak Ridge National Laboratory

51. Na, B.-C., Sartori, E.J.N.s. & engineering (2002). Organization for economic cooperation and development/Nuclear Energy Agency international benchmark on the VENUS-2 MOX core measurements. 142, 37-47.

52. NEA (2002). Chernobyl: Assessment of Radiological and Health Impacts (2002). OECD Publishing, Paris

53. Petit, C., Scudder, T. & Lambin, E.J.I.J.o.R.S. (2001). Quantifying processes of land-cover change by remote sensing: resettlement and rapid land-cover changes in south-eastern Zambia. 22, 3435-3456.

54. Ravanat, J.-L., Douki, T.J.R.P. & Chemistry (2016). UV and ionizing radiations induced DNA damage, differences and similarities. 128, 92-102.

55. Rogan, J. & Chen, D.J.P.i.p. (2004). Remote sensing technology for mapping and monitoring land-cover and land-use change. 61, 301-325.

56. Santos, P., Sillero, N., Boratyński, Z. & Teodoro, A. (2019a). Landscape changes at Chernobyl. In: *Remote Sensing for Agriculture, Ecosystems, and Hydrology XXI*. SPIE, pp. 509-526.

57. Santos, P., Sillero, N.P., Boratyński, Z., Teodoro, A.C.M., Neale, C.M. & Maltese, A. (2019b). Landscape changes at Chernobyl. In: *Remote Sensing for Agriculture, Ecosystems, and Hydrology XXI*.

58. Schmid, S.D. (2015). *Producing power: The pre-Chernobyl history of the Soviet nuclear industry*. MIT Press.

59. Sekizawa, R., Ichii, K. & Kondo, M.J.R.S.L. (2015). Satellite-based detection of evacuation-induced land cover changes following the Fukushima Daiichi nuclear disaster. 6, 824-833.

60. Shcheglov, A., Tsvetnova, O.g. & Klyashtorin, A.J.J.o.G.E. (2014). Biogeochemical cycles of Chernobyl-born radionuclides in the contaminated forest ecosystems. Long-term dynamics of the migration processes. 144, 260-266.

61. Sohl, T., Sleeter, B.J.R.S.o.L.U. & Cover, L. (2012). 15 Role of Remote Sensing for Land-Use and Land-Cover Change Modeling. 225.

62. Tikhomirov, F. & Shcheglov, A.J.S.o.t.T.E. (1994). Main investigation results on the forest radioecology in the Kyshtym and Chernobyl accident zones. 157, 45-57.

63. Tulik, M. & Rusin, A.J.E.p. (2005). Microfibril angle in wood of Scots pine trees (Pinus sylvestris) after irradiation from the Chernobyl nuclear reactor accident. 134, 195-199.

64. Vogelmann, J.E., Tolk, B. & Zhu, Z.J.R.S.o.E. (2009). Monitoring forest changes in the southwestern United States using multitemporal Landsat data. 113, 1739-1748.

65. Xia, Y.J.P.i.M.B. & Science, T. (2020). Correlation and association analyses in microbiome study integrating multiomics in health and disease. 171, 309-491.

66. Wacker, A. & Landgrebe, D.J.L.T.R. (1972). Minimum distance classification in remote sensing. 25.

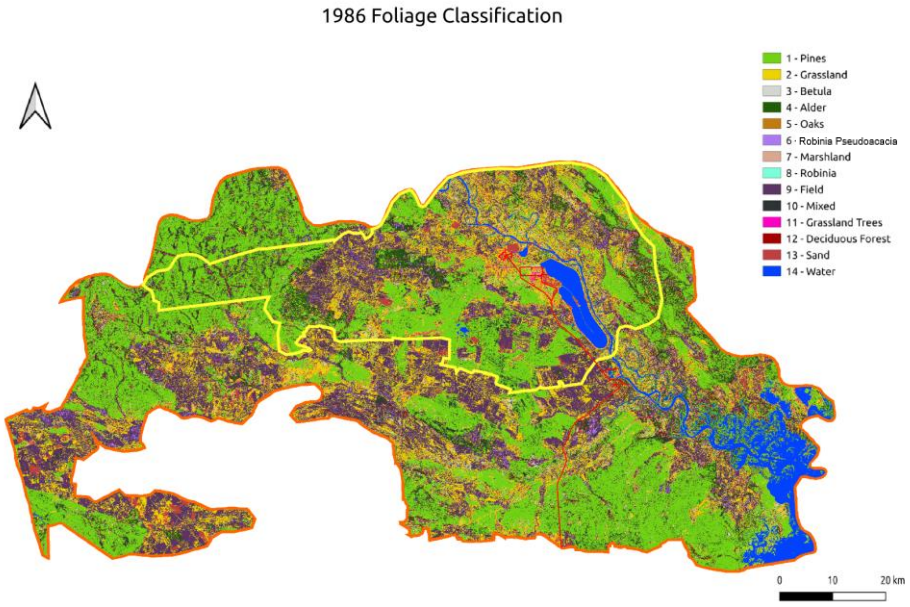
67. Wallace, J., Behn, G., Furby, S.J.E.M. & Restoration (2006). Vegetation condition assessment and monitoring from sequences of satellite imagery. 7, S31-S36.

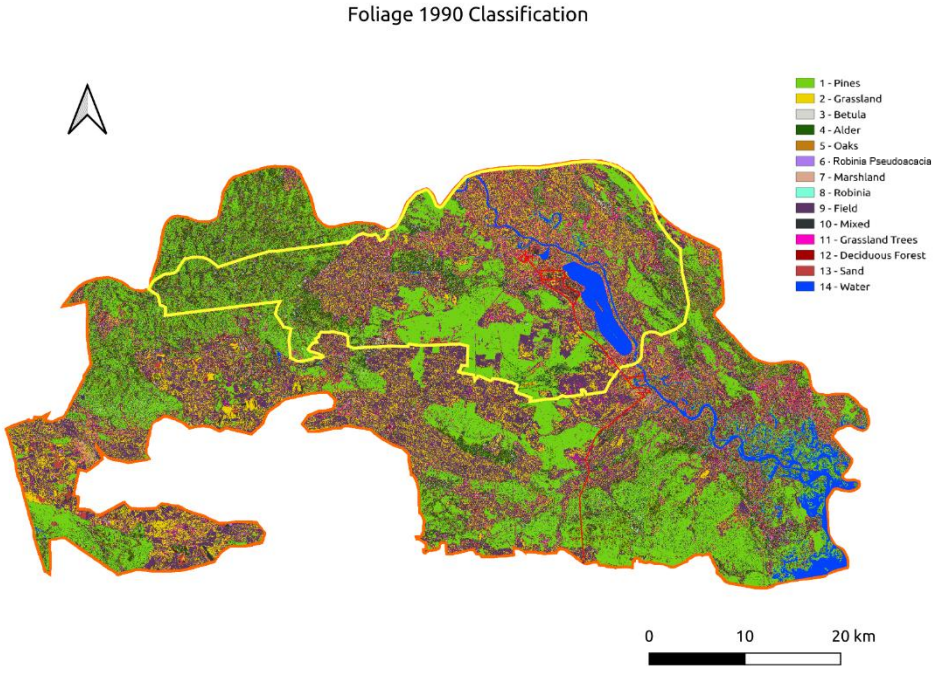
68. Yushchenko, V., Kashparov, V., Protsak, V., Lundin, S., Levchuk, S., Kadygrib, A. *et al.* (2006). Resuspension and redistribution of radionuclides during grassland and forest fires in the Chernobyl exclusion zone: part I. Fire experiments. 86, 143-163.

69. Zhu, Z. & Woodcock, C.E. (2012). Object-based cloud and cloud shadow detection in Landsat imagery. *Remote Sensing of Environment*, 118, 83-94.

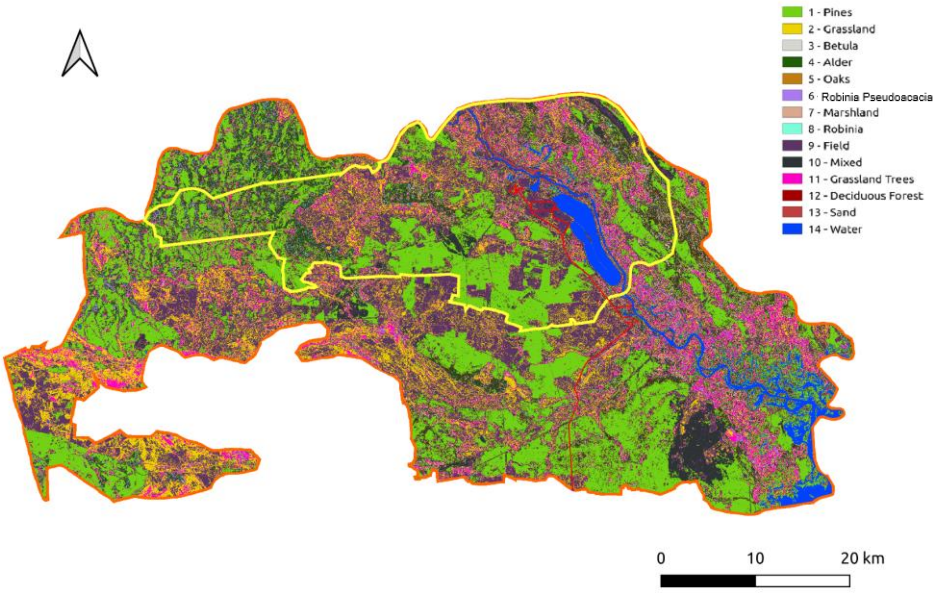
Appendix I

Classified images for each year of the Foliage season dataset

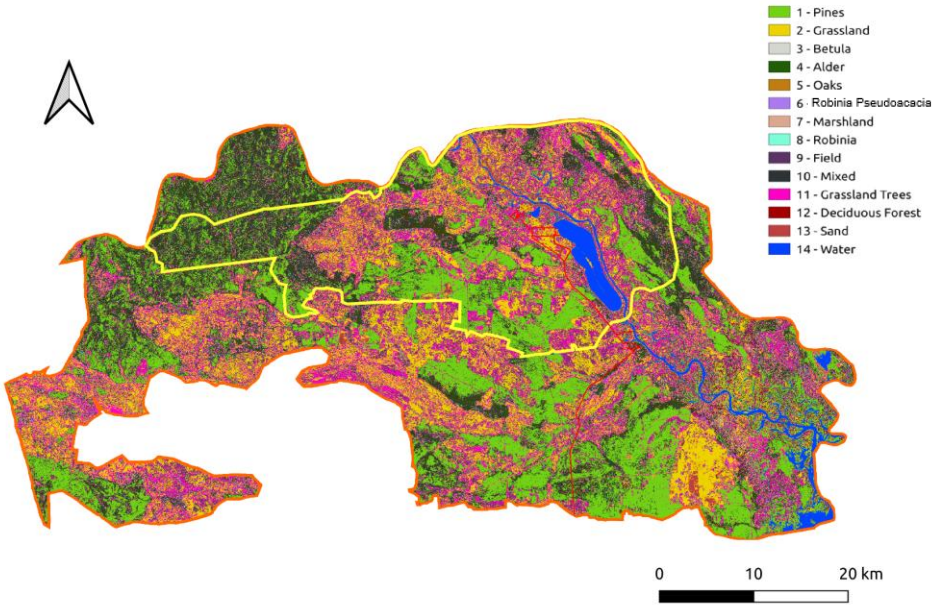


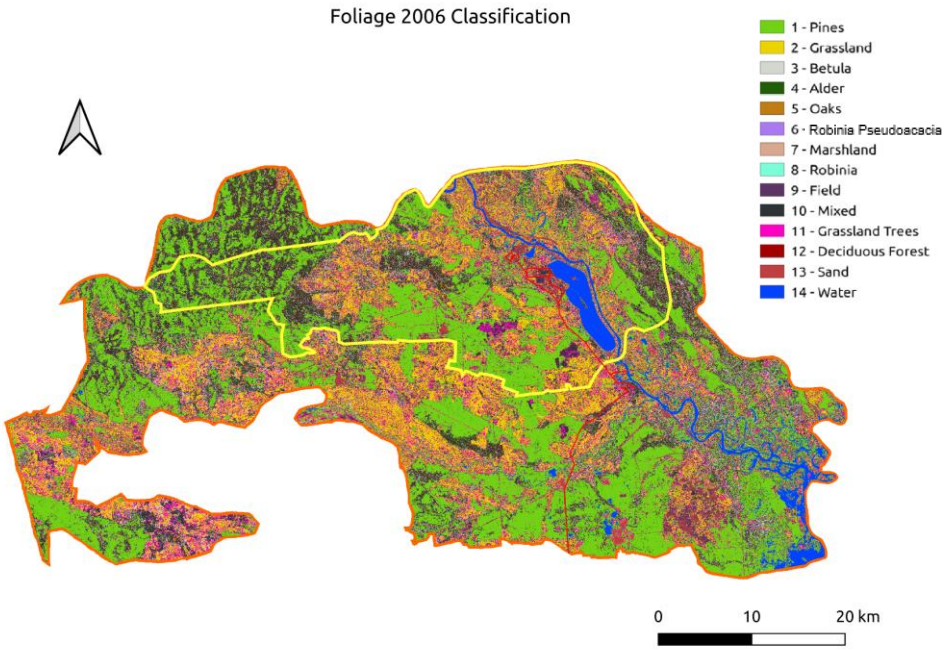


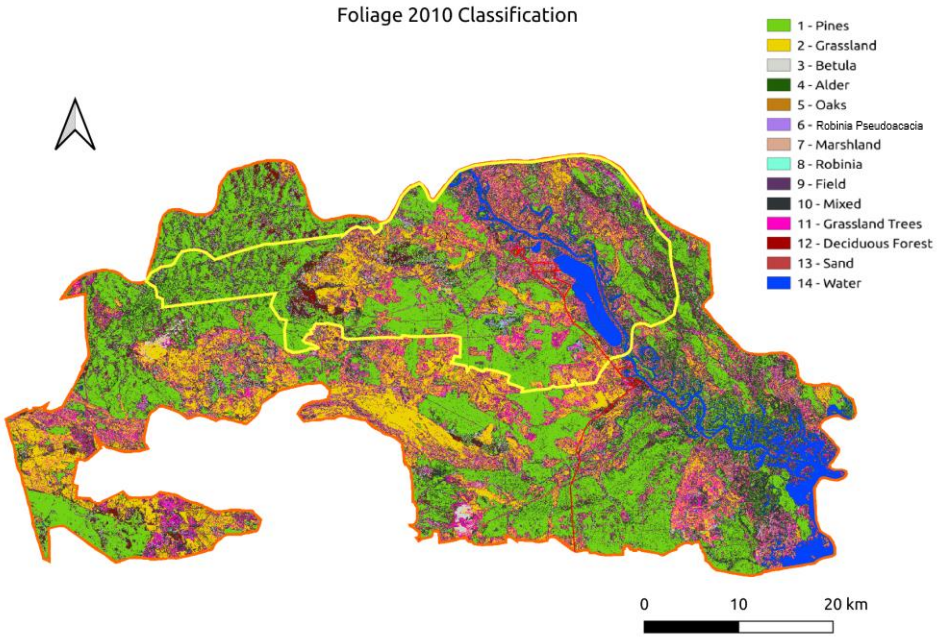
Foliage 1994 Classification

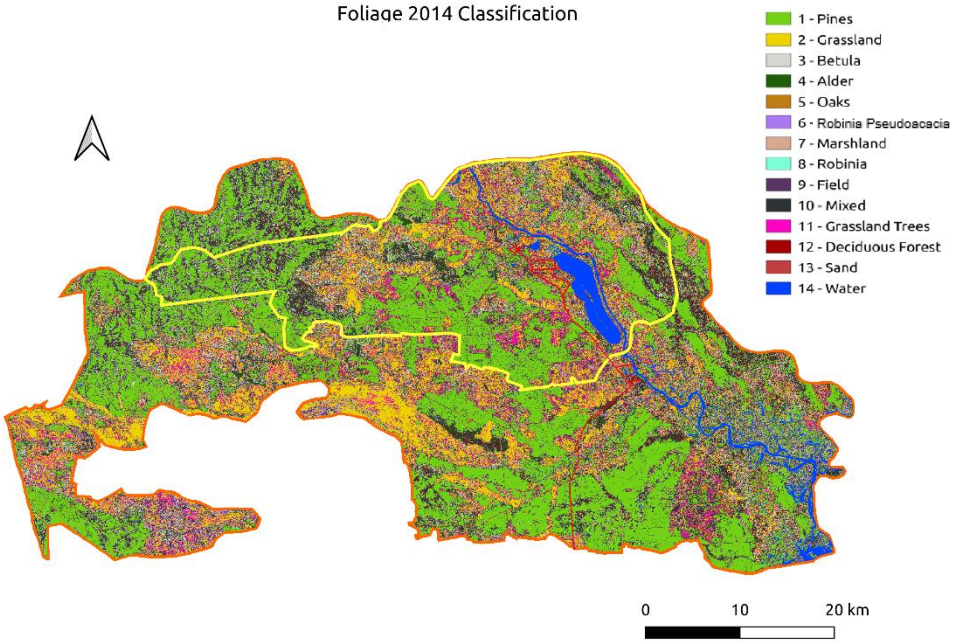


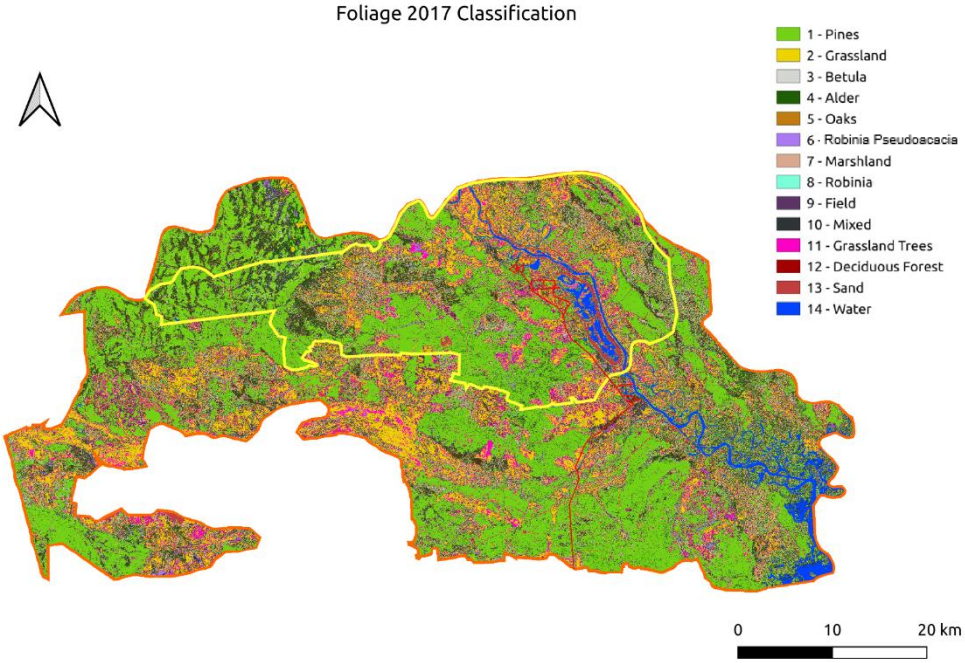
Foliage 2002 Classification




Foliage 2006 Classification
1 - Pines
2 - Grassland
3 - Betula
4 - Alder
5 - Oaks
6 - Robinia Pseudoacacia
7 - Marshland
8 - Robinia
9 - Field
10 - Mixed
11 - Grassland Trees
12 - Deciduous Forest
13 - Sand
14 - Water
0
10
20 km

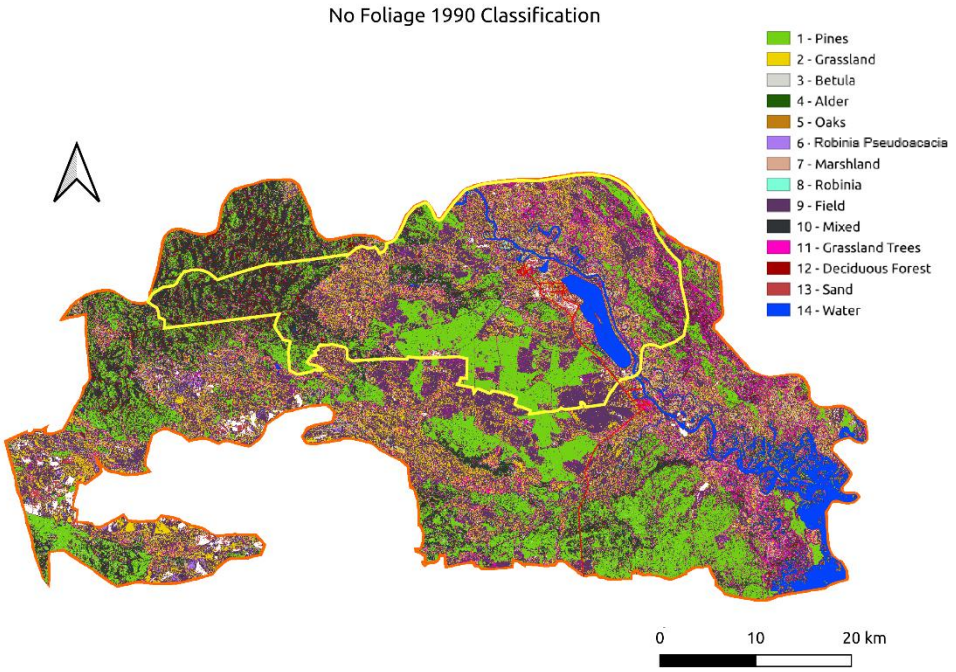

Foliage 2010 Classification
1 - Pines
2 - Grassland
3 - Betula
4 - Alder
5 - Oaks
6 - Robinia Pseudoacacia
7 - Marshland
8 - Robinia
9 - Field
10 - Mixed
11 - Grassland Trees
12 - Deciduous Forest
13 - Sand
14 - Water
0
10
20 km

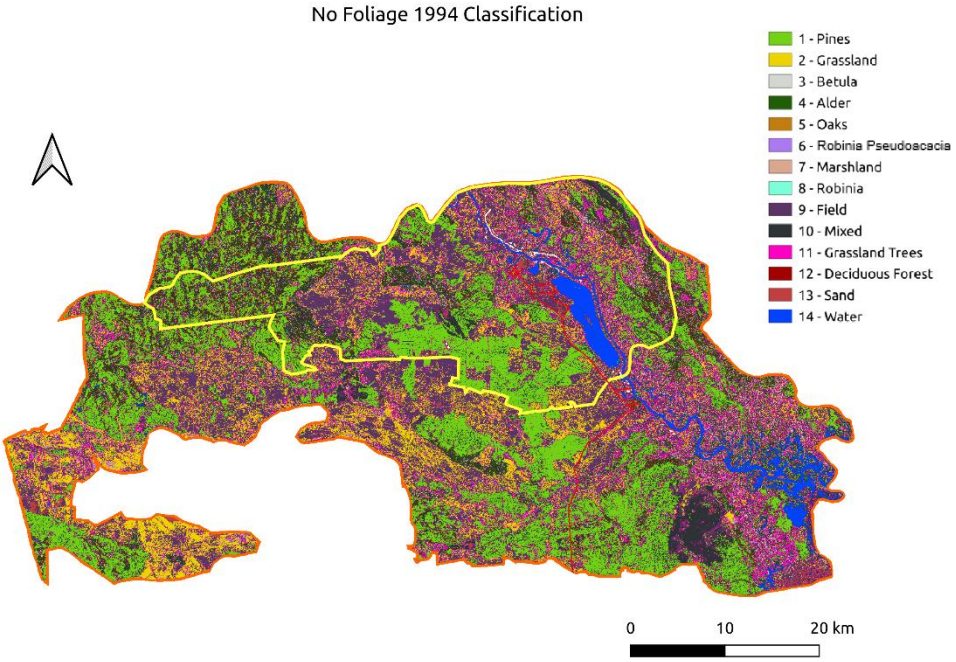

Foliage 2014 Classification
1 - Pines
2 - Grassland
3 - Betula
4 - Alder
5 - Oaks
6 - Robinia Pseudoacacia
7 - Marshland
8 - Robinia
9 - Field
10 - Mixed
11 - Grassland Trees
12 - Deciduous Forest
13 - Sand
14 - Water
0
10
20 km

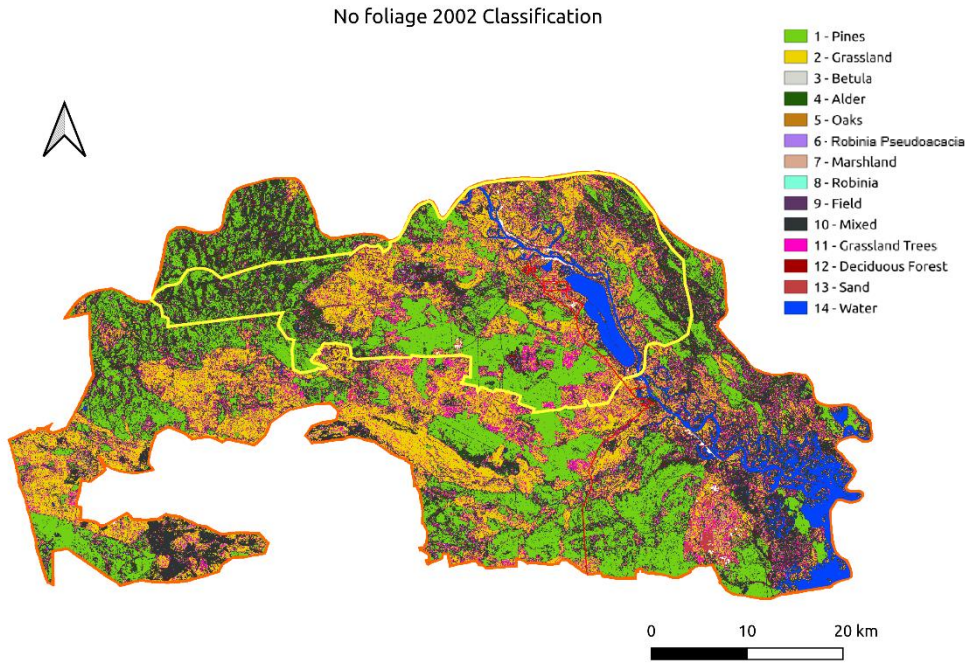

Foliage 2017 Classification
1 - Pines
2 - Grassland
3 - Betula
4 - Alder
5 - Oaks
6 - Robinia Pseudoacacia
7 - Marshland
8 - Robinia
9 - Field
10 - Mixed
11 - Grassland Trees
12 - Deciduous Forest
13 - Sand
14 - Water
0
10
20 km

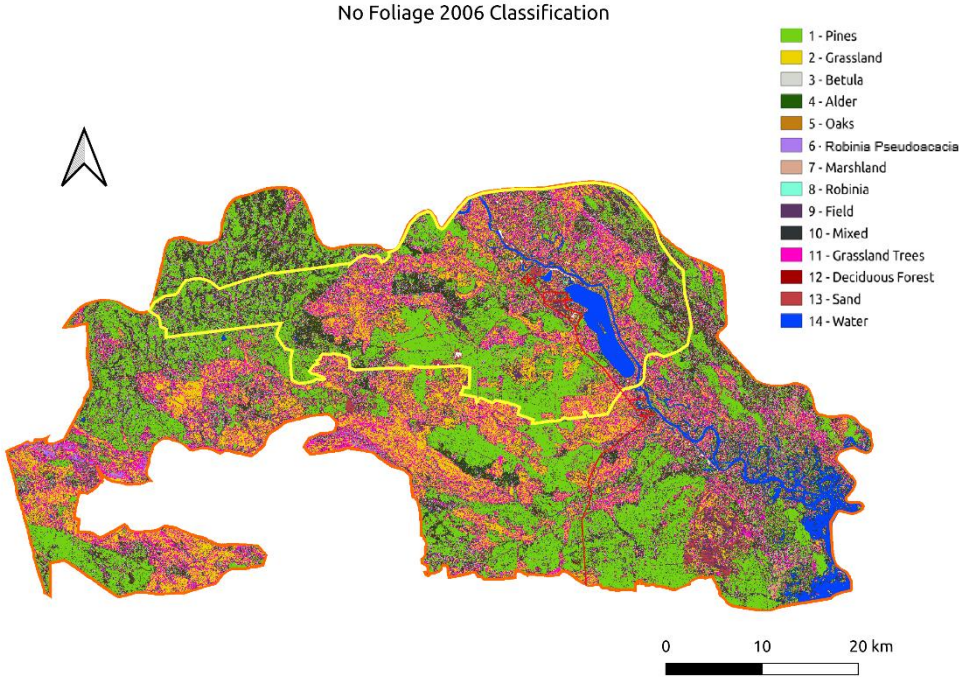
Appendix II

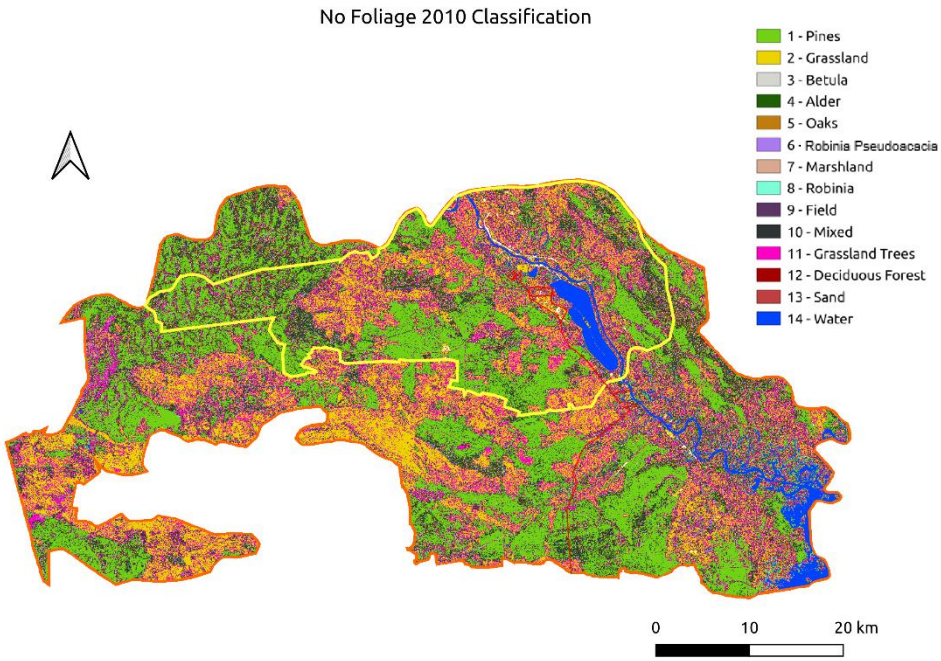
Classified images for each year of the No-Foliage season dataset

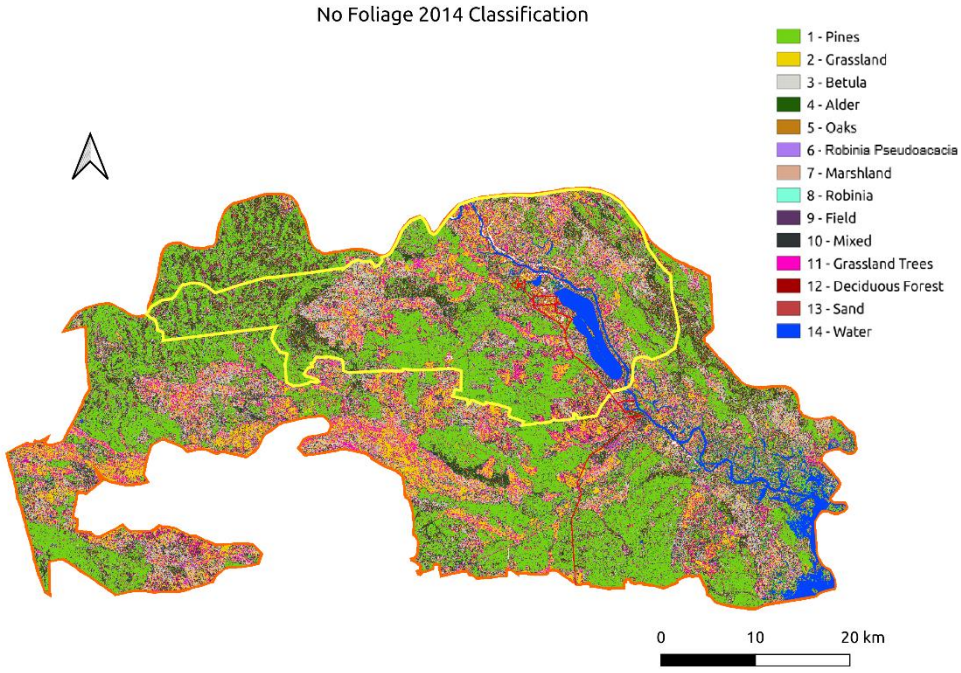


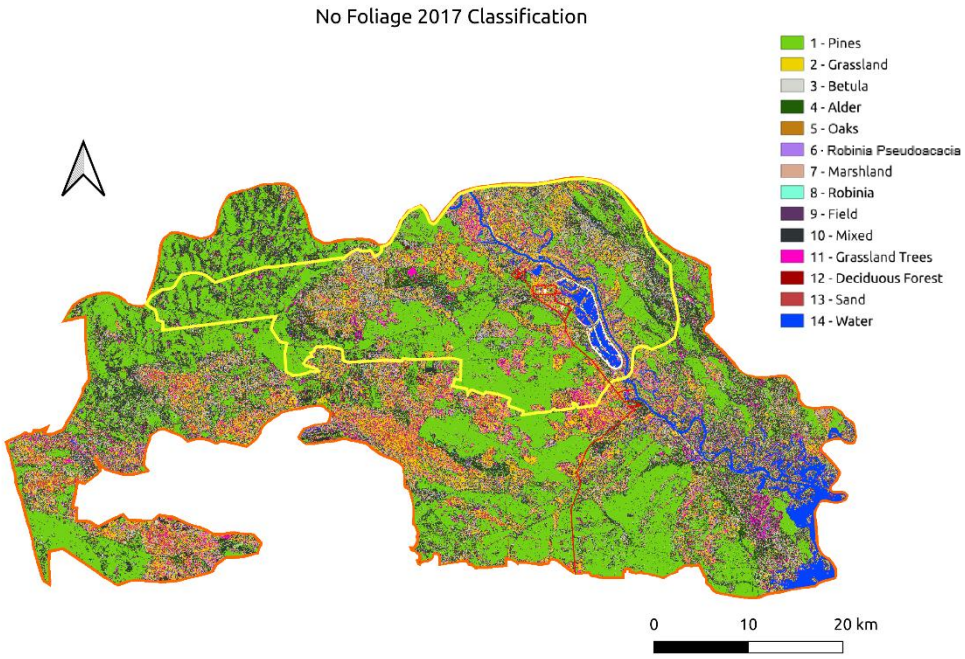



No foliage 2002 Classification
1 - Pines
2 - Grassland
3 - Betula
4 - Alder
5 - Oaks
6 - Robinia Pseudoacacia
7 - Marshland
8 - Robinia
9 - Field
10 - Mixed
11 - Grassland Trees
12 - Deciduous Forest
13 - Sand
14 - Water
0
10
20 km


No Foliage 2006 Classification
1 - Pines
2 - Grassland
3 - Betula
4 - Alder
5 - Oaks
6 - Robinia Pseudoacacia
7 - Marshland
8 - Robinia
9 - Field
10 - Mixed
11 - Grassland Trees
12 - Deciduous Forest
13 - Sand
14 - Water
0
10
20 km

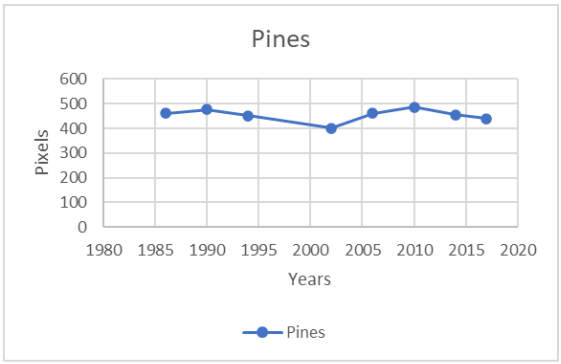

No Foliage 2010 Classification
1 - Pines
2 - Grassland
3 - Betula
4 - Alder
5 - Oaks
6 - Robinia Pseudoacacia
7 - Marshland
8 - Robinia
9 - Field
10 - Mixed
11 - Grassland Trees
12 - Deciduous Forest
13 - Sand
14 - Water
0
10
20 km

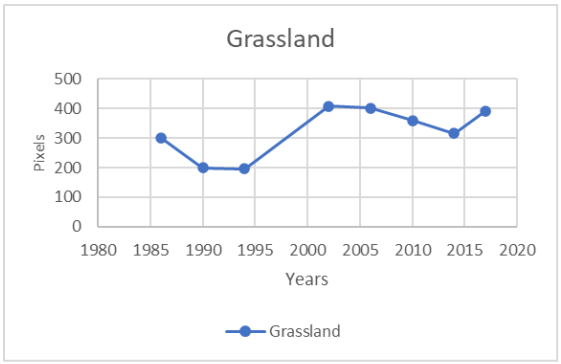

No Foliage 2014 Classification
1 - Pines
2 - Grassland
3 - Betula
4 - Alder
5 - Oaks
6 - Robinia Pseudoacacia
7 - Marshland
8 - Robinia
9 - Field
10 - Mixed
11 - Grassland Trees
12 - Deciduous Forest
13 - Sand
14 - Water
0
10
20 km

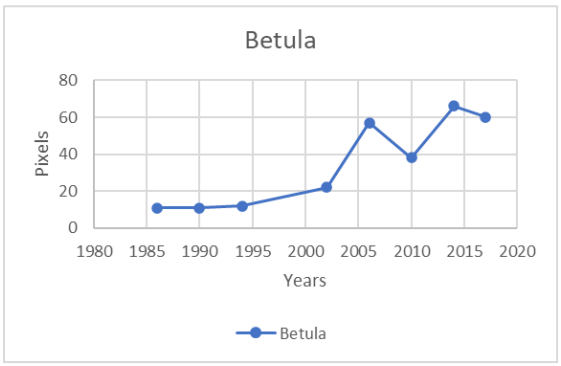

No Foliage 2017 Classification
1 - Pines
2 - Grassland
3 - Betula
4 - Alder
5 - Oaks
6 - Robinia Pseudoacacia
7 - Marshland
8 - Robinia
9 - Field
10 - Mixed
11 - Grassland Trees
12 - Deciduous Forest
13 - Sand
14 - Water
0
10
20 km

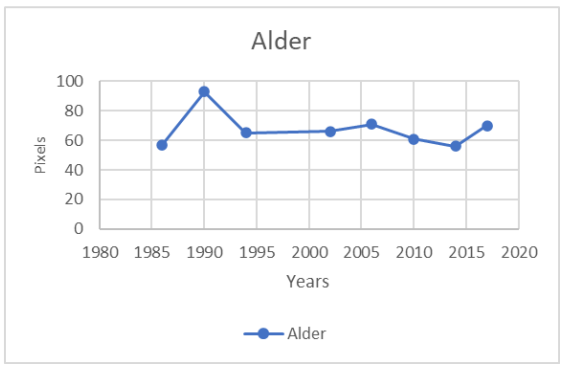
Appendix III

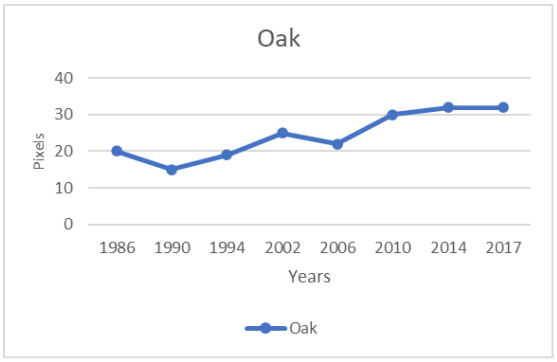
Graphics of the pixels evolution of each individual class over the years of the Foliage dataset

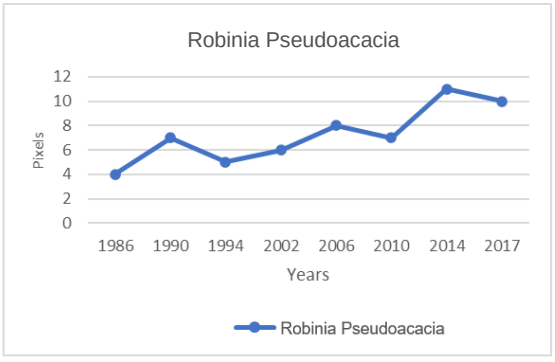


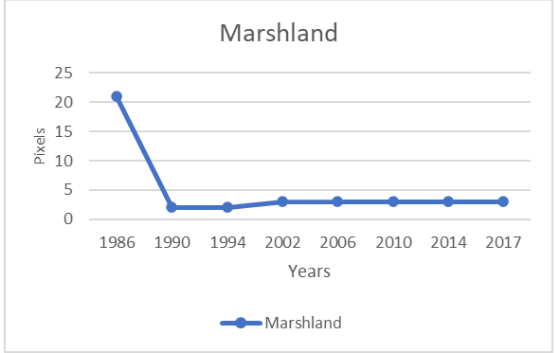


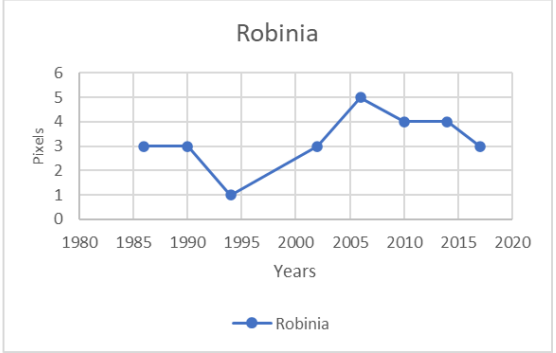


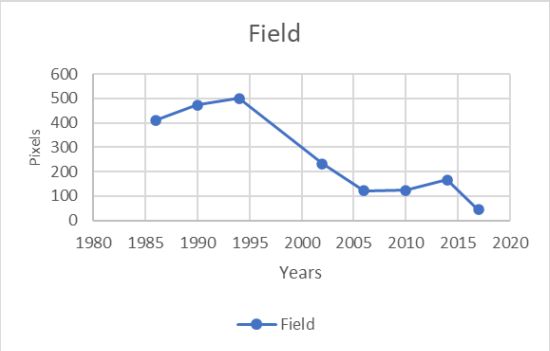


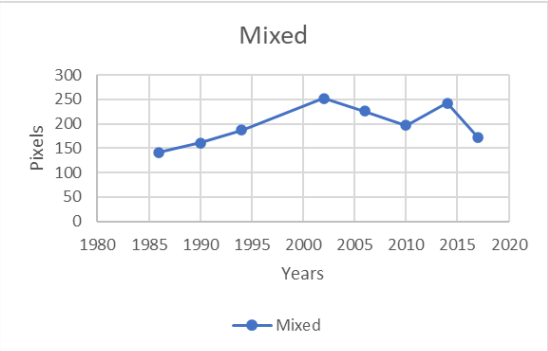


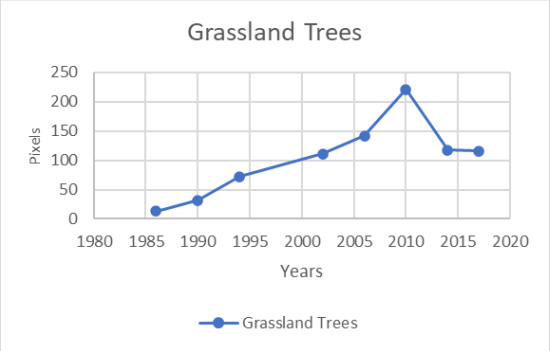


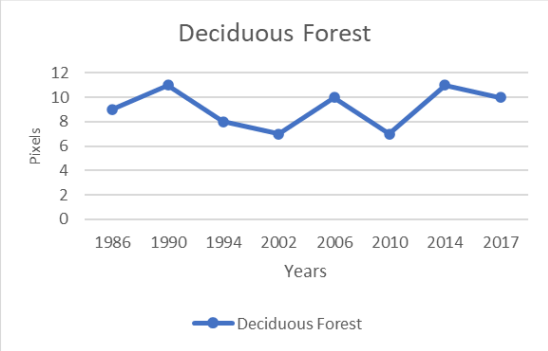





Field
600
500
400
300
200
100
0
Pixels
1980 1985 1990 1995 2000 2005 2010 2015 2020
Years
Field

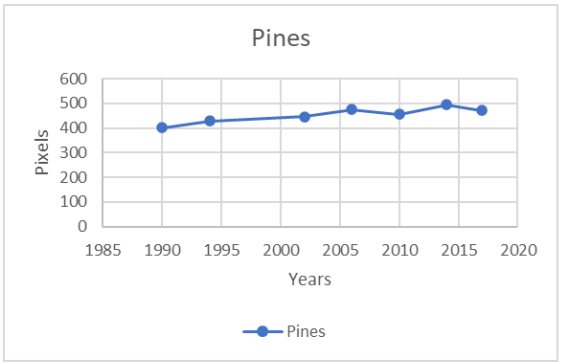

Mixed
300
250
200
150
100
50
0
Pixels
1980 1985 1990 1995 2000 2005 2010 2015 2020
Years
Mixed

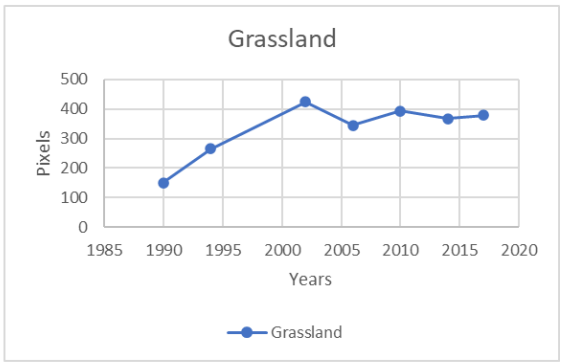

Grassland Trees
250
200
150
100
50
0
Pixels
1980 1985 1990 1995 2000 2005 2010 2015 2020
Years
Grassland Trees

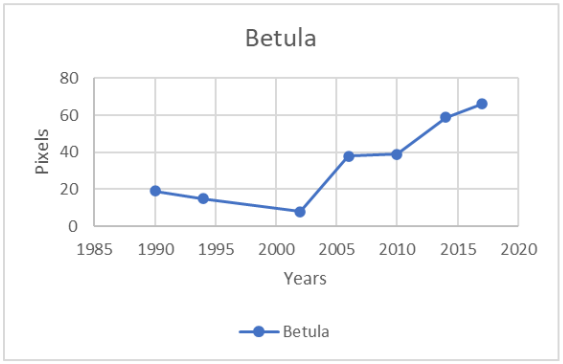

Deciduous Forest
12
10
8
6
4
2
0
Pixels
1986 1990 1994 2002 2006 2010 2014 2017
Years
Deciduous Forest

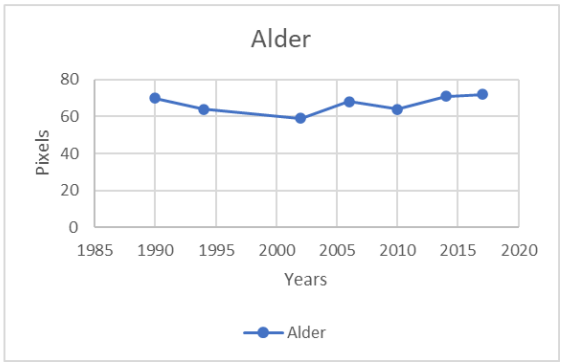
Appendix IV

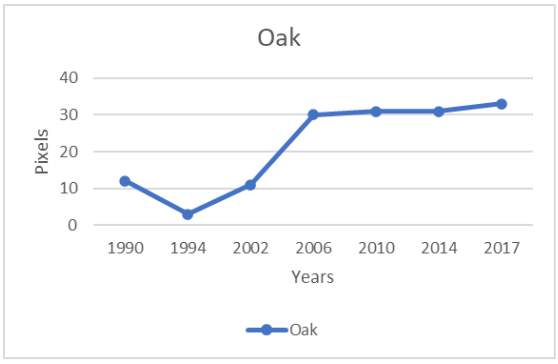
Graphics of the pixels evolution of each individual class over the years of the No-Foliage dataset

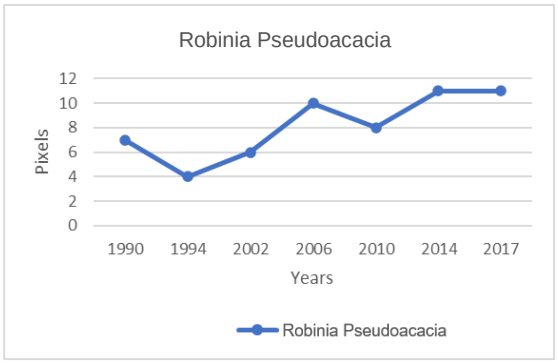


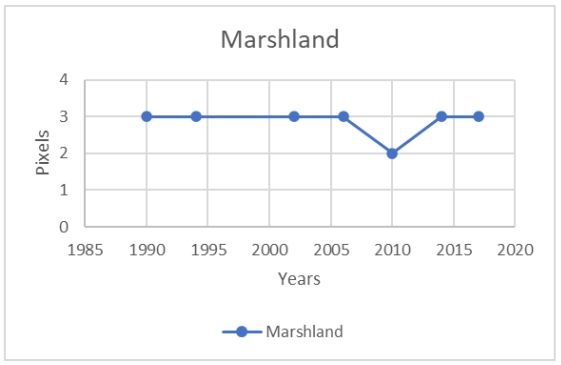


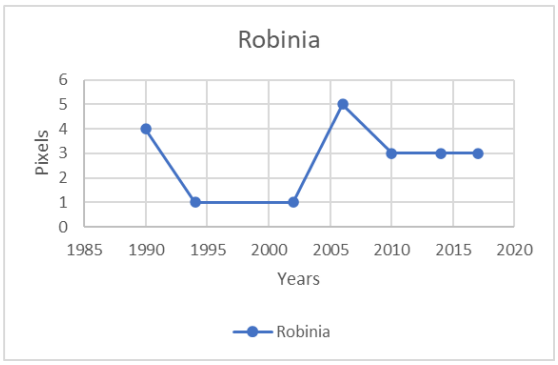


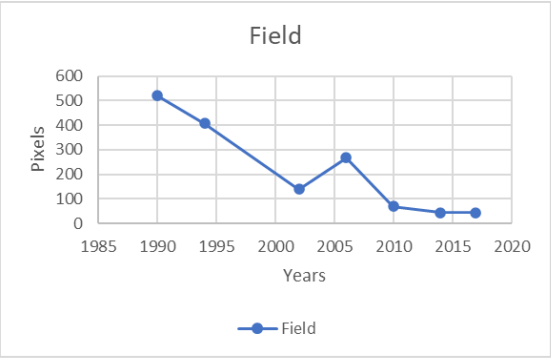


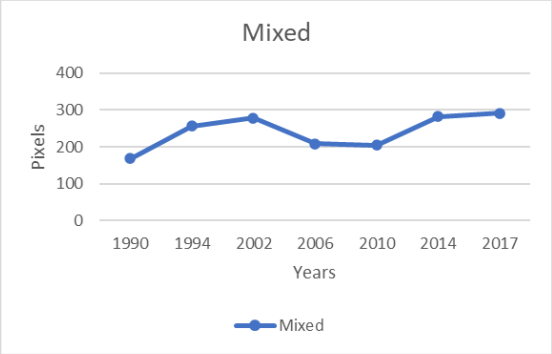


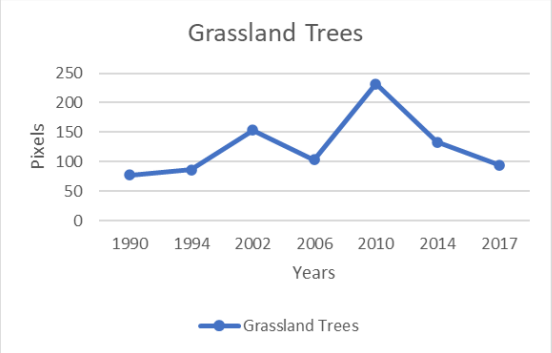


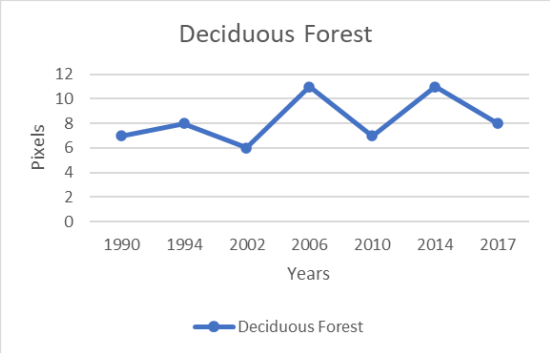





Field
600
500
400
300
200
100
0
Pixels
1985
1990
1995
2000
2005
2010
2015
2020
Years
Field


Mixed
400
300
200
100
0
Pixels
1990
1994
2002
2006
2010
2014
2017
Years
Mixed


Grassland Trees
250
200
150
100
50
0
Pixels
1990
1994
2002
2006
2010
2014
2017
Years
Grassland Trees


Deciduous Forest
12
10
8
6
4
2
0
Pixels
1990
1994
2002
2006
2010
2014
2017
Years
Deciduous Forest